Journal of Medicinal Chemistry

Subscriber access provided by UNIV OF SCIENCES PHILADELPHIA

Article

Discovery of Trifluoromethyl Glycol Carbamates as Potent and Selective Covalent Monoacylglycerol Lipase (MAGL) Inhibitors for Treatment of Neuroinflammation

Laura A. McAllister, Christopher R. Butler, Scot Mente, Steven V. O'Neil, Kari R. Fonseca, Justin R. Piro, Julie A. Cianfrogna, Timothy L. Foley, Adam M. Gilbert, Anthony R. Harris, Christopher J. Helal, Douglas S. Johnson, Justin I. Montgomery, Deane M Nason, Stephen Noell, Jayvardhan Pandit, Bruce N. Rogers, Tarek A. Samad, Christopher L. Shaffer, Rafael Guimaraes da Silva, Daniel P. Uccello, Damien Webb, and Michael A. Brodney

J. Med. Chem., **Just Accepted Manuscript** • DOI: 10.1021/acs.jmedchem.8b00070 • Publication Date (Web): 02 Mar 2018

Downloaded from http://pubs.acs.org on March 3, 2018

Just Accepted

"Just Accepted" manuscripts have been peer-reviewed and accepted for publication. They are posted online prior to technical editing, formatting for publication and author proofing. The American Chemical Society provides "Just Accepted" as a service to the research community to expedite the dissemination of scientific material as soon as possible after acceptance. "Just Accepted" manuscripts appear in full in PDF format accompanied by an HTML abstract. "Just Accepted" manuscripts have been fully peer reviewed, but should not be considered the official version of record. They are citable by the Digital Object Identifier (DOI®). "Just Accepted" is an optional service offered to authors. Therefore, the "Just Accepted" Web site may not include all articles that will be published in the journal. After a manuscript is technically edited and formatted, it will be removed from the "Just Accepted" Web site and published as an ASAP article. Note that technical editing may introduce minor changes to the manuscript text and/or graphics which could affect content, and all legal disclaimers and ethical guidelines that apply to the journal pertain. ACS cannot be held responsible for errors or consequences arising from the use of information contained in these "Just Accepted" manuscripts.

ACS Publications

Journal of Medicinal Chemistry is published by the American Chemical Society. 1155 Sixteenth Street N.W., Washington, DC 20036

Published by American Chemical Society. Copyright © American Chemical Society. However, no copyright claim is made to original U.S. Government works, or works produced by employees of any Commonwealth realm Crown government in the course of their duties.

SCHOLARONE™
Manuscripts

Discovery of Trifluoromethyl Glycol Carbamates as Potent and Selective Covalent Monoacylglycerol Lipase (MAGL) Inhibitors for Treatment of Neuroinflammation

Laura A. McAllister*[a], Christopher R. Butler[a], Scot Mente[a], Steven V. O'Neil[b], Kari R. Fonseca[a], Justin R. Piro[a], Julie A. Cianfrogna[b], Timothy L. Foley[b], Adam M. Gilbert[b], Anthony R. Harris[b], Christopher J. Helal[b], Douglas S. Johnson[a], Justin I. Montgomery[b], Deane M. Nason[b], Stephen Noell[b], Jayvardhan Pandit[b], Bruce N. Rogers[a], Tarek A. Samad[a], Christopher L. Shaffer[a], Rafael G. da Silva[b] Daniel P. Uccello[b], Damien Webb[a], and Michael A. Brodney[a].

[a]Pfizer Worldwide Research and Development, 610 Main St, Cambridge, MA, 02139, United States; [b] Pfizer Worldwide Research and Development, 445 Eastern Point Road, Groton, CT, 06340, United States.

KEYWORDS: Monoacylglycerol Lipase, MAGL, neuroinflammation, covalent inhibitors

ABSTRACT Monoacylglycerol lipase (MAGL) inhibition provides a potential treatment approach to neuroinflammation through modulation of both the endocannabinoid pathway, and arachidonoyl signaling in the central nervous system (CNS). Herein we report the discovery of compound **15** (PF-06795071), a potent and selective covalent MAGL inhibitor, featuring a novel trifluoromethyl glycol leaving group which confers significant physicochemical property improvements as compared with earlier inhibitor series with more lipophilic leaving groups. The design strategy focused on identifying an optimized leaving group that delivers MAGL potency,

serine hydrolase selectivity, and CNS exposure; while simultaneously, reducing LogD, improving solubility, and minimizing chemical lability. Compound **15** achieves excellent CNS exposure, extended 2-AG elevation effect *in vivo*, and decreased brain inflammatory markers in response to an inflammatory challenge.

Introduction

Monoacylglycerol lipase (MAGL) is a serine hydrolase which regulates the endocannabinoid pathway and arachidonoyl signaling in the central nervous system (CNS) (Figure 1a).[1-6] Emerging biological data suggests that inhibiting MAGL may be a promising therapeutic approach to multiple diseases, particularly those in which neuroinflammation plays a central role.[7-10] Neuroinflammation occurs as a consequence of disease or injury resulting in activation of resident immune cells (microglia and astrocytes), production of pro-inflammatory cytokines and chemokines, and deterioration of the blood brain barrier.[11] Persistent neuroinflammation can result in neuronal death and ultimately contribute to neurodegeneration.[12] Inhibition of MAGL has therefore been proposed as a potential therapeutic approach for Alzheimer's disease (AD),[13] Parkinson's disease (PD),[14] multiple Sclerosis (MS),[15] pain and acute brain injury.[16-19]

MAGL is highly expressed throughout the body, including the brain, liver and lungs. In the brain, MAGL has a central role in controlling levels of the endocannabinoid 2-arachidonylglycerol (2-AG), and the pro-inflammatory eicosanoid precursor arachidonic acid (AA).[20] MAGL catalyzes the transformation of 2-AG to AA (Figure 1b), which can be further converted to pro-inflammatory eicosanoids. MAGL serves as the primary regulator of AA in the brain, controlling >85% of 2-AG metabolism, in contrast to the periphery, where AA is primarily derived from phospholipids via cytosolic phospholipase A2 (cPLA2). Arachidonic acid (AA) is

also utilized by COX enzymes for the synthesis of inflammatory prostaglandins and thromboxanes, thus lowering AA levels results in further anti-inflammatory effects. Moreover, MAGL is located presynaptically at axon terminals, and co-localized with the cannabinoid receptor 1 (CB1). As a potent CB1/2 agonist, 2-AG activates the endocannabinoid system, which has been reported to have beneficial impact on inflammation.[21] Therefore, this dual role in controlling neuroinflammation through central 2-AG and AA regulation supports wide ranging therapeutic potential for MAGL inhibitors.

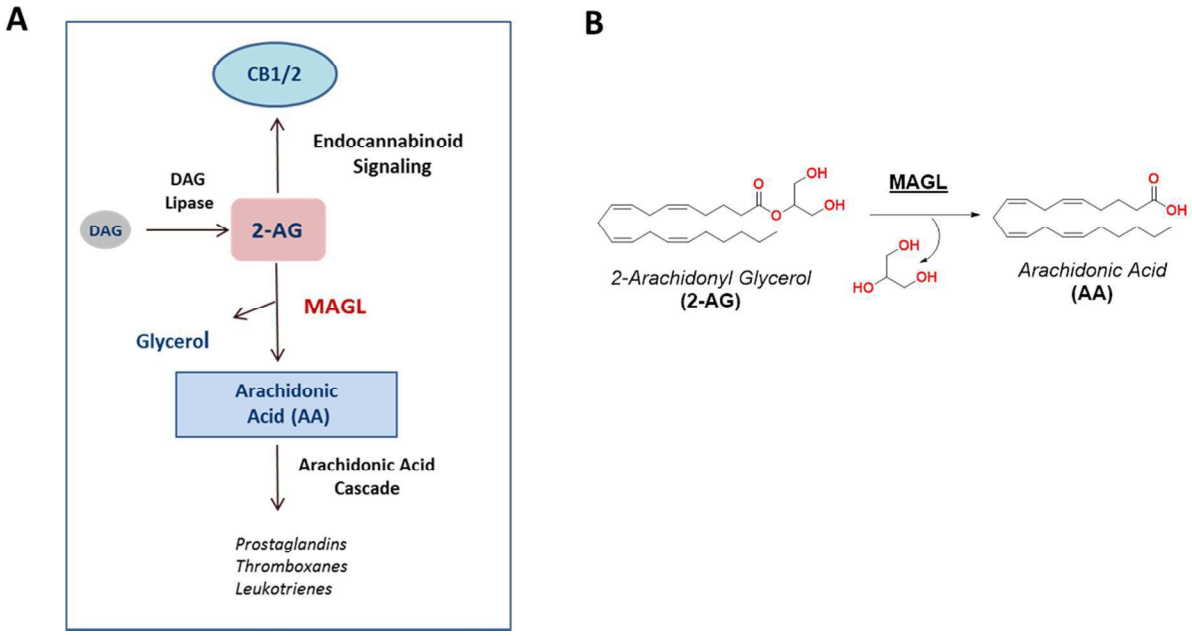

Figure 1. (a) 2-AG plays a central role in endocannabinoid pathway signaling and arachidonyl inflammatory cascade in the brain. (b) MAGL catalyzes the hydrolytic conversion of 2-arachidonyl glycerol (2-AG) to arachidonic acid (AA).

MAGL is a membrane bound serine hydrolase, tethered intracellularly by an anchoring α-helical region.[22] The substrate binding site comprises a large hydrophobic tunnel which forms the acyl-chain binding region (ACB pocket), accommodating the long aliphatic chain of the natural

substrate 2-AG. At the head of the ACB pocket is a catalytic triad of amino acids (Ser122, His269 and Asp239). The triad activates Ser122, which nucleophilically attacks the carbonyl of 2-AG. An oxyanion hole, comprised of two backbone amide residues in this region, stabilizes the developing negative charge on the carbonyl in the transition state en route to the tetrahedral intermediate during catalysis. Beyond the catalytic triad is the cytoplasmic access channel (CA channel), that consists of more polar residues, ultimately leading to the cytoplasm. The polar residues of this channel complement the hydrophilic glyceryl moiety of 2-AG, and upon hydrolysis, the expelled glycerol molecule presumably exits the enzyme via this channel.

A covalent inhibition approach is one strategy to deliver sustained inhibition of MAGL at a feasible human dose.[23] This approach was deemed to be the most viable for achieving good MAGL potency, and the high levels of sustained inhibition that were targeted for efficacy in neuroinflammatory conditions. Reversible inhibitors of MAGL with sub-micromolar potency have been recently reported.[24-25] However, a reversible profile is desirable when the objective is to achieve more transient MAGL blockade. In addition, achieving the desired MAGL potency in a desirable property space has proved challenging with reversible inhibitors. Several series of covalent MAGL inhibitors have emerged in the last decade, and some representative examples are shown in Figure 2a.[26-36] A typical feature of these inhibitors is an amine core linking to a lipophilic tail region, needed to complement the lipophilic ACB pocket. The amine core is capped with a carbamate or urea head group featuring a leaving group, which is generally an alcohol or heterocycle. [22] This moiety presumably binds in the CA channel of the active site, or "leaving group pocket" prior to covalent modification. Upon binding of the inhibitor to the MAGL active site, Ser122 attacks the carbonyl carbon, triggering leaving group departure. This

results in a stable adduct with the core and tail region of the inhibitor molecule, rendering the enzyme incapable of further degradation of 2-AG (Figure 2b).

The hydrophobic nature of a large section of the MAGL binding pocket demands significant lipophilicity for binding and inhibition. To complement the highly lipophilic nature of the ACB pocket, many potent inhibitors reside in a highly lipophilic space (cLogP > 4). As a result, these compounds often have poor solubility, making evaluation of *in vivo* efficacy and further development challenging. Moreover, metabolic clearance also increases with lipophilicity, which leads to higher requisite doses to achieve efficacy. Molecules in these higher cLogP ranges are also considered non-ideal because of their higher propensity for associated off-target promiscuity and safety risks.[37]

A common motif employed in reported covalent MAGL inhibitors is the hexafluoroisopropanol (HFIP) leaving group (Figure 2a, compounds **1-3**). This group confers a favorable potency and selectivity profile, providing a balance between the levels of reactivity required for reaction with Ser122 at the MAGL active site, with low enough inherent chemical lability to avoid promiscuous serine hydrolase inhibition. However, a major disadvantage of this moiety is its high lipophilicity, which exacerbates the already requisite lipophilic regions of the ACB pocket. This has the potential to result in compounds with high clogP, which often correlates with high clearance and poor solubility.

The development of MAGL inhibitors that could treat neuroinflammation resulting from acute traumatic or non-traumatic brain injury would potentially require delivery via intravenous (IV) route of administration. To that end, our goal was to develop highly soluble MAGL inhibitors for the treatment of these acute neurological conditions. Incorporation of the HFIP moiety would increase the challenge of achieving such a profile, with the resulting compounds having

unfavorably high clogP, poor solubility, high clearance, and poor lipophilic efficiency (LipE).[38] We sought to identify a new series of brain penetrant MAGL inhibitors with improved solubility, and thus more amenable to IV formulation. The requirement to reduce LogD to improve solubility needed to be balanced with the requirement to avoid transporter liabilities (PgP and BCRP) to maintain good CNS penetration.[39] Since the MAGL pocket contains more polar residues in the region corresponding to the leaving group binding pocket (the CA channel), the design strategy focused on modifying the leaving group to effectively balance these properties. A further objective in the design of the leaving group was to engender potency from a balance of target-specific binding efficacy and reactivity, rather than simple non-specific chemical reactivity.[40] Minimizing inherent chemical reactivity of the carbamate is one approach to avoid indiscriminate reactivity with other off-target proteins, and to optimize selectivity for MAGL versus other related serine hydrolases (e.g. fatty acid amide hydrolase (FAAH)). A further consideration associated with covalent approaches, which is simultaneously addressed by minimizing chemical reactivity, is the desire to mitigate the risk of idiosyncratic adverse drug reactions (IADRs). It has been reported that minimizing total daily covalent body burden (via low dose), and reducing the intrinsic electrophilic activity may contribute to reducing IADR safety risks in covalent drugs.[41-44]

Herein we report the identification of compound **15** (PF-06795071), a covalent MAGL inhibitor featuring a novel, stereodefined, trifluoromethyl glycol leaving group. This compound shows a comparable potency and selectivity profile to compounds containing the more lipophilic and chemically labile HFIP leaving group. This compound shows significantly improved solubility compared with earlier leads, improving the feasibility of our objective of a MAGL inhibitor suitable for IV dosing. Compound **15** shows excellent selectivity against FAAH and

other serine hydrolases, demonstrates good brain penetration, and a clean *in vitro* safety profile. Furthermore, compound **15** is efficacious in sustaining elevation of 2-AG levels *in vivo*, and in reducing markers of neuroinflammation in animal models.

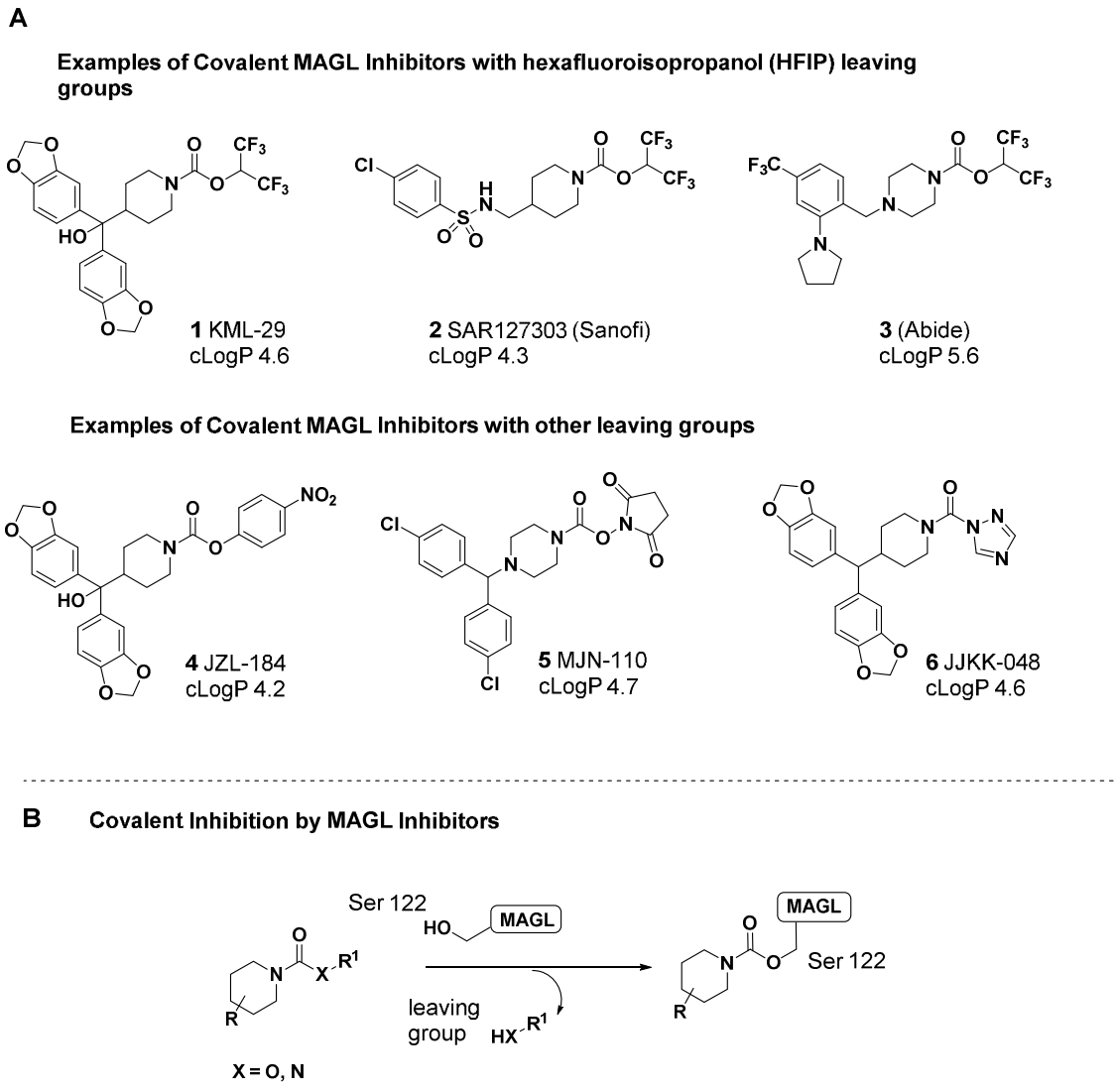

Figure 2. (a) Representative examples of covalent MAGL Inhibitors with the heaxfluoroisopropanol (HFIP) and other leaving groups. (b) MAGL inactivation by covalent inhibitors.

Results and Discussion

We previously reported a series of pyrazole azetidine analogs such as compound **7** (Figure 3), displaying excellent MAGL potency (MAGL IC_{50} = 0.3 nM) and a good selectivity profile.[45] An expectation of irreversible MAGL inhibitors is that one should observe an extended *in vivo* pharmacodynamic (PD) effect of MAGL inhibition (raised 2-AG levels). Upon testing analogs from this azetidine series in mouse *in vivo* PK/PD studies, we observed only a transient elevation in 2-AG. Cellular activity based protein profiling (ABPP) studies confirmed that this class of compounds covalently inhibited MAGL transiently and led us to speculate that the azetidine adducts formed at the MAGL site are rapidly hydrolyzed from the enzyme. We observed that analogs containing larger ring cores, such as piperidines, resulted in improved MAGL adduct stability and thus prolonged PD effects.

Recent efforts to optimize the core system of these inhibitors resulted in the discovery of compounds based on a [3.1.0] bicyclic core system, such as compound **8** (Figure 3). Compound **8** retains MAGL potency (MAGL IC_{50}= 1.4 nM) and has excellent FAAH selectivity (FAAH IC_{50} = 4.3 μM, Table 1). Despite a promising pharmacology profile, compound **8** resides in a high LogD space, and has poor kinetic solubility (< 1μM). To address these challenges, we systematically explored leaving groups with the goal of improving drug-like properties. To this end, a series of analogs that varied the alcohol leaving group in lower LogD space was prepared (Table 1).

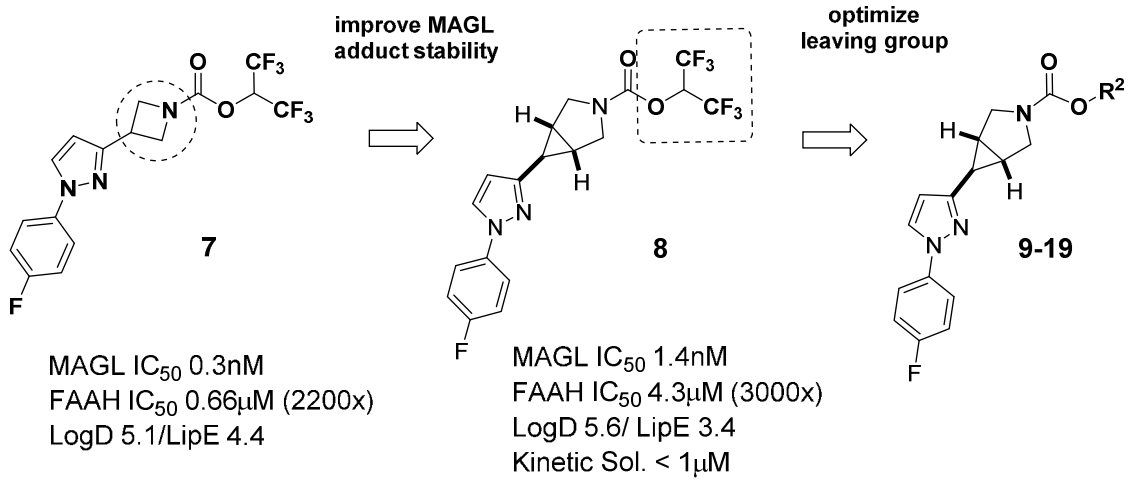

Figure 3. Design of MAGL Inhibitors with improved adduct stability and lower LogD

Synthesis of MAGL Inhibitor Leaving Group Analogs. Synthesis of analogs based upon the [3.1.0] system core with various leaving groups was achieved using the general strategy outlined in Scheme 1. Beginning with Boc-protected 3-azabicyclo[3.1.0]hexane-6-carboxylic acid **20**, the carboxylic acid group was converted to the corresponding methyl ketone **21** via Weinreb amide formation and Grignard addition. Subsequent conversion to pyrazole **22**, followed by copper-catalyzed N-arylation with 4-fluorophenyl boronic acid afforded Boc-protected N-aryl pyrazole compound **23**. Removal of the Boc protecting group provided the key amine intermediate **24**. The reaction of **24** with an activated carbonate or chloroformate derived from an appropriate alcohol (corresponding to the desired leaving group) afforded the analogs in Table 1 and 2.

Scheme 1. Synthesis of carbamate analogs in Table 1 and 2

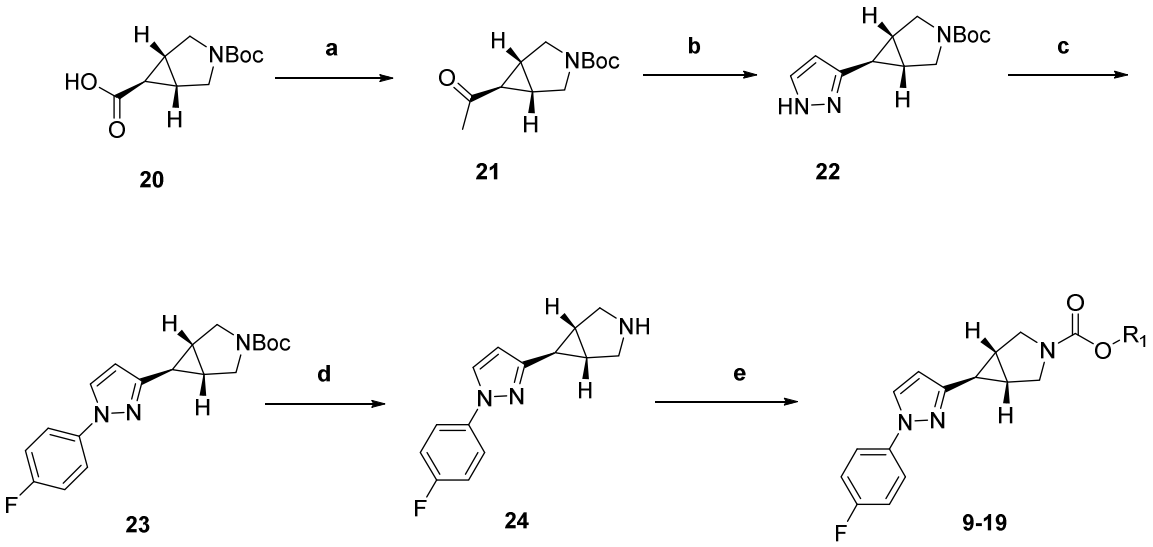

(a) i. NHMeOMe.HCl, EDCI, HOBT, DIPEA, CH_2Cl_2, 0 ^oC; ii. MeMgBr, THF, 0 ^oC, 99% over 2 steps; (b) i. DMF-DMA, DMF, 110 ^oC; ii. NH_2NH_2, EtOH, 80 ^oC, 16 h, 94%; (c) 4-F phenylboronic acid, $Cu(OAc)_2$, pyridine, 4Å MS, CH_2Cl_2, 30 ^oC, 18h, 60%; (d) CF_3CO_2H, rt.; (e) chloroformates or activated carbonates .

In vitro Assays. MAGL potency was evaluated *in vitro* by measuring inhibition of turnover of a fluorogenic substrate (7-HCA, 7-hydroxycoumarinyl arachidonate) by recombinant MAGL, following 30 minute incubation with inhibitors.[46] While this method allows for rank ordering of potency, results are dependent on pre-incubation time. k_{inact}/K_I ratios were measured for more accurate characterization of irreversible inhibition; a greater k_{inact}/K_I value indicates a more effective inhibitor.[47] k_{inact}/K_I ratio accounts for binding efficiency of the entire inhibitor molecule in the pre-covalent state (within the K_I parameter), as well as the rate of the covalent attachment step (within k_{inact}). k_{inact}/K_I values for MAGL inhibitors shown in Table 1 correlate well with respective IC_{50} measurements. FAAH inhibition potency was assessed using

recombinant FAAH and a fluorescent substrate (arachidonoyl-AMC), following a 30 minute pre-incubation with compounds.

Structure Activity Relationships. Table 1 shows the impact of combining various leaving groups with compounds based on a [3.1.0] bicyclic core system on MAGL inhibition profile and properties. As a reference, several analogs containing the literature alcohol leaving groups were evaluated (compounds **8-10**). The calculated pK_a of the leaving group alcohol was used as an indicator of relative chemical reactivity of the groups. Compound **8** with hexafluoroisopropanol (HFIP) as the leaving group showed excellent MAGL potency (IC_{50} = 1 nM) and selectivity versus FAAH (IC_{50} = 4.3 μM). In contrast, while the *p*-nitrophenol-derived analog **9** is potent at MAGL (IC_{50} = 24 nM), it lacks selectivity over FAAH (IC_{50} = 18 nM). The N-hydroxysuccinimidyl carbamate **10** is significantly less potent despite greater reactivity to HFIP. A potential explanation may be less favorable binding of this group in the CA pocket.

Using the HFIP alcohol as a starting point, small modifications to reduce LogD were designed and prepared. Replacement of one trifluoromethyl group with a simple methyl in compound **11** resulted in a significant potency reduction (MAGL IC_{50} = 242 nM), likely attributable to reduced reactivity of this group as suggested by the pK_a. Interestingly, acceptable FAAH selectivity levels were largely maintained (4300 fold for **8** vs > 95 fold for **11**). Removal of the branched alkyl group altogether resulted in a simple trifluoroethyl leaving group in compound **12** that exhibited significantly reduced MAGL potency, and interestingly resulted in significant erosion of FAAH selectivity. Comparison of compound **11** and **12** would suggest that branching in the leaving group pocket is an important structural feature for maintaining selectivity over FAAH. This is consistent with an earlier report on the affinity of anandamide analogs for rat anandamide amino hydrolase, where branched analogs disfavored binding.[48] Encouragingly, compound **13**

which contains a tetra-fluorinated leaving group, corresponding to one LogD unit reduction in lipophilicity relative to **11**, regained potency at MAGL (IC_{50} = 26 nM) and maintained FAAH selectivity (73 fold).

With these results in hand, and inspired by the structure of the natural substrate for MAGL (2-AG), we designed compound **14**, in which one highly lipophilic trifluoromethyl group is replaced with a more polar hydroxyl group, resulting in a LogD reduction of almost two units (Figure 4). It was postulated the polar "OH" group should be tolerated in this region of the CA pocket, since the glycerol moiety in 2-AG can bind in this region. Gratifyingly, we observed that racemic glycol analog **14** retained excellent potency at MAGL (IC_{50} = 6 nM), excellent selectivity against FAAH (>2000-fold), and improved lipophilic efficiency [38] (LipE = 4.3) as compared with the HFIP analog **8** (LipE 3.4).

Table 1. Leaving Group SAR

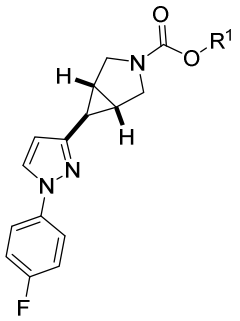

Compound	-OR_1	MAGL IC_{50} (nM)[a]	k_{inact}/K_I ($M^{-1}s^{-1}$)[b]	FAAH IC_{50} (μM)[c]	LogD[d]	LipE[f]	Leaving Group pKa[g]
4	-	5.6	16173	>11	5.1	3.1	7.2
7	-	0.33	650964	0.66	5.1	4.4	9.8
8	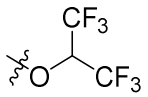	1	41708	4.3	5.6	3.4	9.8
9	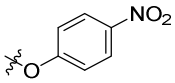	24	2879	0.018	4.2[e]	3.4	7.2
10	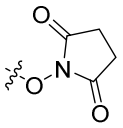	46	156	3.6	2.6[e]	4.7	7.8
11	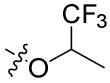	242	ND	>23	4.8	1.8	12.5
12	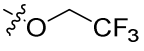	445	103	0.97	4.2	2.2	12.5
13	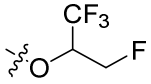	26	1578	1.9	4.3	3.3	11.2
14	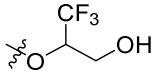	6	12966	14	3.9	4.3	11.7

[a]IC_{50} values measured from MAGL inhibition assay. Activity measured after 30 min pre-incubation with compound. Values represent the geometric mean of at least three experiments. 95% confidence intervals are provided in the supporting information. [b] k_{inact}/K_I ratio. [c]IC_{50} values measured from FAAH inhibition assay. Values represent the geometric mean of at least three experiments. [d]Measured eLogD values. eLogD is an HPLC based method for measuring LogD[49]. [e]SFLogD measured at pH 7.4[50]. [f]Lipophilic efficiency (LipE) defined as MAGL pIC_{50}-LogD. [g]Calculated pK_a of alcohol leaving group (ACD labs).

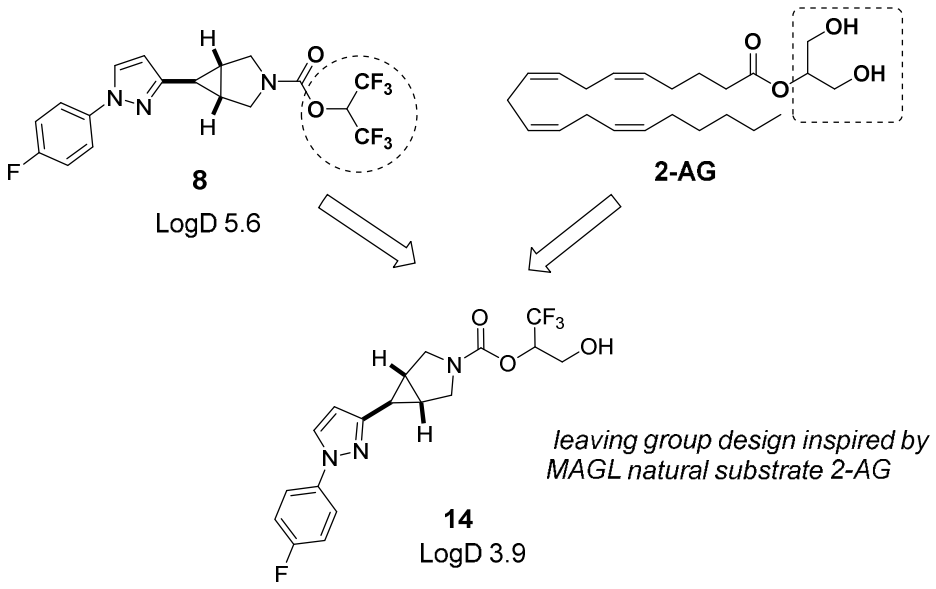

Figure 4. Design of glycol moiety in compound **14** inspired by 2-AG, the natural substrate of MAGL.

Encouraged by the promising profile of compound **14**, closely related analogs of **14** were synthesized and profiled, as shown in Table 2. Separating enantiomers afforded the more active compound **15**, which had the expected improvement in potency (MAGL IC_{50} 3 = nM, k_{inact}/K_I = 29,724 $M^{-1}s^{-1}$) consistent with a positive binding interaction with the pocket. Enantiomer **16** was less potent (MAGL IC_{50} = 890 nM), which reinforced the suggestion that the MAGL inhibition did not predominantly result from leaving group reactivity alone (wherein the enantiomers would exhibit the same potency), but rather by making a positive binding interaction in the pocket. Capping the hydroxyl group with a methyl group (compound **17)**, or homologating the glycol to position the hydroxyl further from the carbamate (compound **18**) results in a significant potency drop. Modifying the position of trifluoromethyl substituent on the glycol (compound **19**) also diminishes MAGL activity. The glycol leaving group in compound **15** was an intriguing advance, because it attained similar levels of MAGL inhibition to compound **8**, despite the glycol leaving group (pK_a = 11.7) being significantly less reactive than the hexafluoroisopropanol in **8**

(pK_a = 9.8). We postulated that the hydroxyl group therefore made a favorable binding interaction in the leaving group pocket in the pre-covalent binding step, relative to the HFIP.

It was postulated that the pK_a of the alcohol could be used as a leading indicator of potency, as it is a reflection of inherent reactivity. To understand the relationship between MAGL pIC_{50} versus the pK_a of the leaving groups, a number of analogs in the series were plotted (Figure 5). For most analogs, MAGL potency (pIC_{50}) correlates with pK_a of the leaving group, with more acidic leaving groups having greater potency. This trend indicates that electrophilicity of the carbamate carbonyl (correlating with pK_a) is the major driving force for potency, and suggests no specific interaction (beneficial or detrimental) of the molecule with the leaving group pocket. In the case of active glycol enantiomer **15**, MAGL inhibition potency is greater than would be expected for this pK_a range.

In addition to desirable MAGL potency, compound **15** retains good selectivity over FAAH (>1000-fold), good lipophilic efficiency (LipE = 4.7), and is in a more desirable property space (LogD = 3.8) than its HFIP analog (**8,** LogD = 5.6). Encouragingly, **15** had an apparent kinetic solubility of 115 μM at pH 7.4, which was a considerable enhancement compared with compound **8** with apparent kinetic solubility of <1 μM at the same pH. A crystalline form of compound **15** had a thermodynamic solubility of 25 μM at pH 6.5 (after 24 h). Furthermore, we were encouraged that compound **15** could potentially have low *in vivo* clearance as oxidative turnover in human liver microsomes is low (HLM Cl_{int} < 8 ml/min/kg).

Table 2. SAR of Trifluoromethyl Glycol Related Analogs

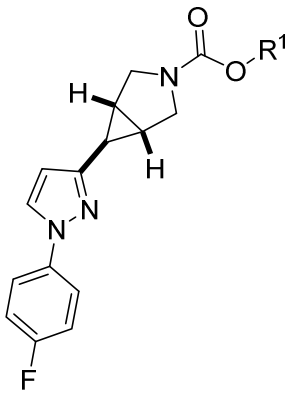

Compound	-OR$_1$	MAGL IC$_{50}$ (nM)[a]	k_{inact}/K_I ($M^{-1}s^{-1}$)[b]	FAAH IC$_{50}$ (μM)[c]	LogD[d]	LipE[e]	HLM CL$_{int}$ (mL/min/kg) [f]
15	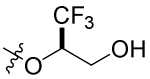	3	29724	3.1	3.8	4.7	<8
16	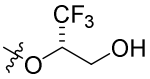	890	79	26	3.9	2.2	<8
17	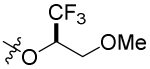	354	110	1.94	4.2	2.3	nd[g]
18	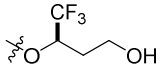	582	4573	>12	4.2	2.0	<12
19	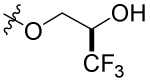	132	244	>30	4.0	2.9	9.4

[a]IC$_{50}$ values measured from MAGL inhibition assay. Activity measured after 30 min pre-incubation with compound. Values represent the geometric mean of at least three experiments. 95% confidence intervals are provided in the supporting information. [b] k_{inact}/K_I ratio. [c]IC$_{50}$ values measured from FAAH inhibition assay. Values represent the geometric mean of at least three experiments. [d]Measured eLogD values. eLogD is an HPLC based method for measuring LogD. [e]Lipophilic efficiency (LipE) defined as MAGL pIC$_{50}$-LogD. [f] Scaled intrinsic clearance in human liver microsomes. [g] nd = not determined

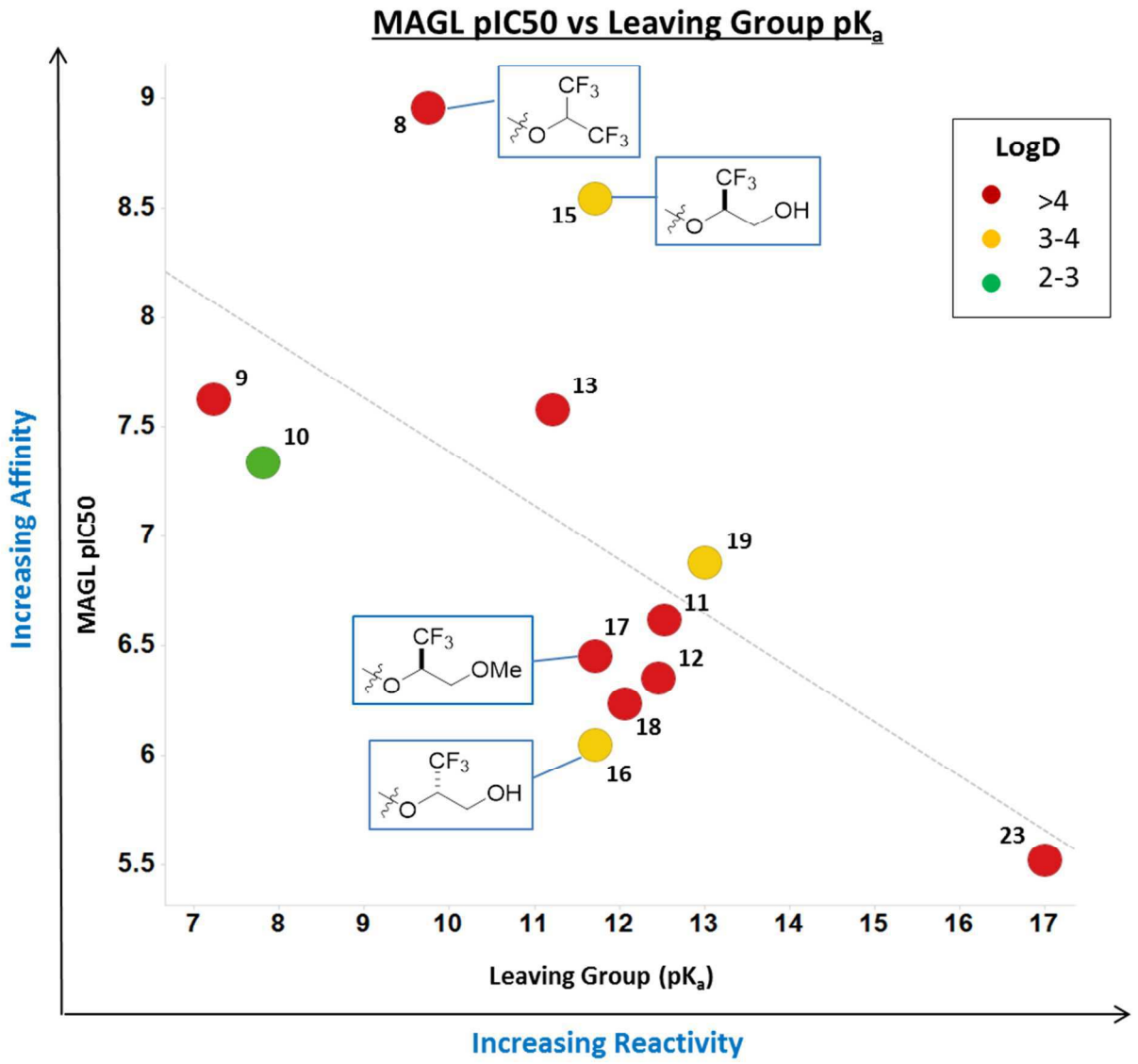

Figure 5. MAGL pIC_{50} of inhibitors from the [3.1.0] series vs pKa of alcohol leaving group.

Asymmetric Synthesis of Compound 15. In order to further profile compound **15**, an efficient asymmetric synthetic route to the glycol leaving group was developed**.** This synthetic route is outlined in Schemes 2 and 3. The initial synthesis of PMB-protected chiral glycol **27** was achieved by nucleophilic addition of *p*-methyoxylbenzyl alkoxide to commercially available racemic epoxide **25** followed by chiral chromatography (Scheme 2). Alternatively, racemic epoxide **25** can be resolved using a Jacobsen hydrolytic kinetic resolution reaction, to give the

desired enantioenriched *(R)* epoxide (**26**) in >98% ee.[51] Ring opening of chiral epoxide **26** with *p*-methyoxylbenzyl alcohol affords the desired enantiomer of **27** without the need for chiral chromatography.

Scheme 2. Synthetic route to protected chiral glycol intermediate

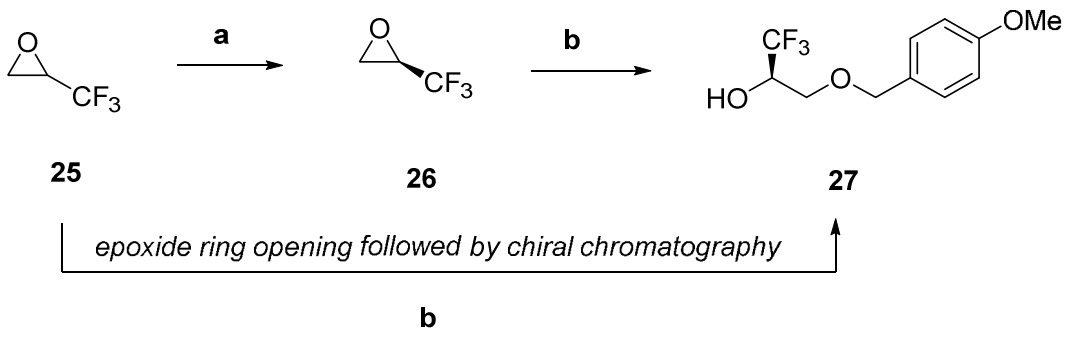

(a) (S,S)-(Salen)Co(III)acetate complex, 0.45 equiv. H_2O, then distillation (>98% ee *(R)*); (b) *p*-methoxybenzyl alcohol, NaHMDS, THF, 41% (**25** to **27**).

With chiral glycol intermediate in hand, compound **15** can be synthesized as outlined in Scheme 3. PMB protected alcohol **27** can be converted to the NHS activated carbonate **28** as shown in Scheme 3, by activation with *N,N'*-disuccinimyl carbonate. Coupling the NHS activated carbonate intermediate **28** to the pyrazole amine **24** and subsequent PMB deprotection provided desired compound **15** in excellent yield.

Scheme 3. Synthesis of compound **15**

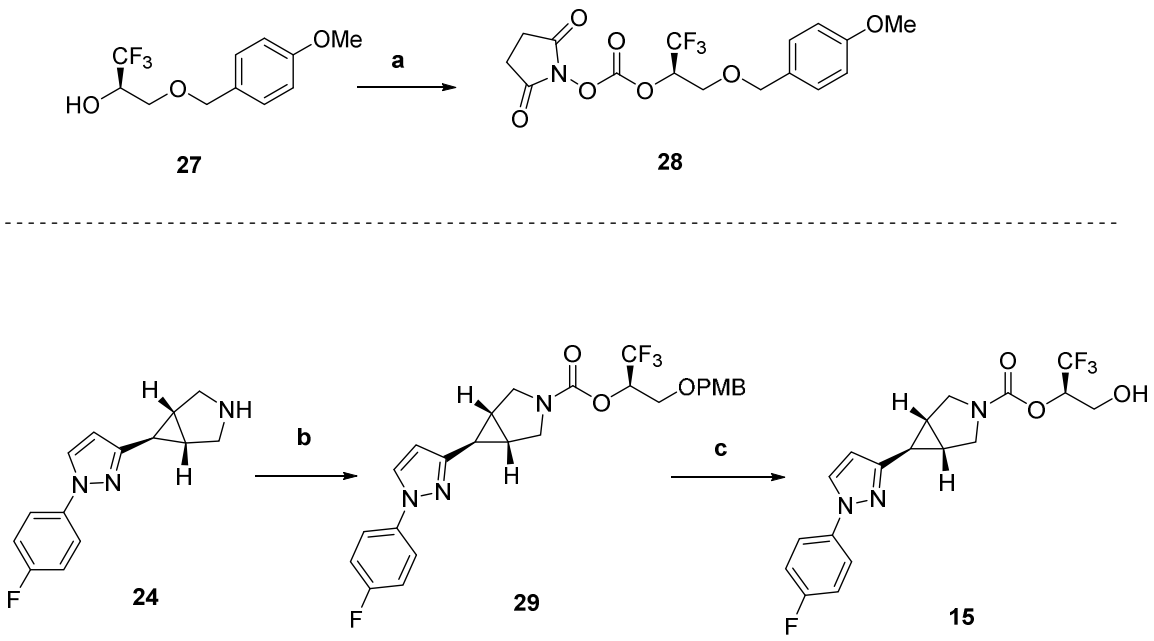

(a) N,N'-disuccinimyl carbonate, NEt_3, CH_2Cl_2, 18h, 25 ^oC (in situ); (b) **28**, CH_2Cl_2, rt, 18h, 61% over 2 steps; (c) CF_3CO_2H, rt., 4h, 65%.

X-Ray Co-crystal structures and MAGL Docking Models. Irreversible modification of MAGL by this series of inhibitors was confirmed through x-ray co-crystal structures. Figure 6 illustrates a MAGL co-crystal structure obtained following treatment with NHS carbamate **10**. The structure confirmed covalent modification of Ser122 in the active site by the inhibitor and demonstrates that the [3.1.0] core with aryl pyrazole tail of the inhibitor complements the shape of the lipophilic MAGL acyl chain binding (ACB) pocket. Although we did not attempt to co-crystalize compound **15** itself with MAGL, we inferred covalent modification of MAGL by compound **15** from its time-dependent inhibition profile in vitro assay systems, and assume an identical adduct is formed to that with compound **10**.

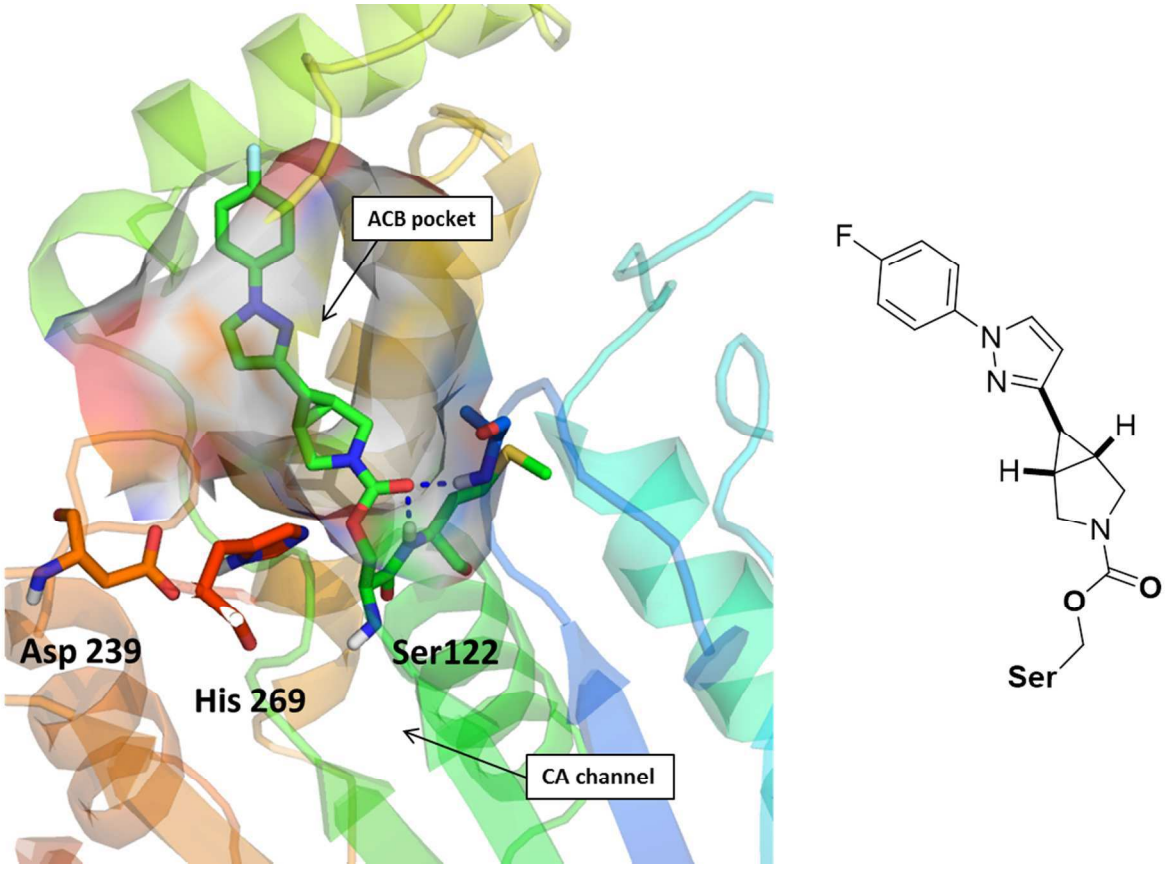

Figure 6. X-ray co-crystal structure of compound **10** bound to MAGL. Crystal structure shows a post-covalent modification snapshot of binding in the MAGL pocket, with leaving group no longer attached (PDB Accession code: 6BQ0).

Unfortunately, co-crystal structures were not helpful in prospectively guiding structure-based design of the leaving group, as the leaving group has already departed in the snapshot of the protein in a post-covalent modification state. Therefore, in order to understand binding and drive leaving group design, molecular modeling efforts focusing on the construction of a "pre-covalent" MAGL-ligand complex were pursued. This was accomplished via modeling of compound **15** into the x-ray structure with the catalytic Ser122 repositioned to that of the published non-covalent MAGL-ligand complex (PDB: 3PE6). The approximate positioning of

the leaving group was then found via docking[52] and subsequent minimization in this MAGL active site.

Docking of compound **15** into the MAGL site with Ser122 placed in the pre-covalent state is shown in Figure 7a and 7b (rotated view). The docked "pre-covalent" compound **15** is shown in green sticks, and can be compared to the X-ray of the post-covalent state shown in purple lines. Here the carbonyl (facing away in Figure 7a, visible in Figure 7b) is oriented toward the two backbone NH donors of Ala51 and Met123, which forms the oxyanion hole. In these docking poses, the carbonyl-NH distance is closer (2.1 Å) for the Ala51 interaction compared to the Met123 (3.1 Å) due to the steric blocking of Ser122. Presumably, as the reaction proceeds to the transition state, the distance from the Ser122 oxygen to the ligand carbon will decrease, and the second oxyanion interaction distance will also shorten. In the structure of the covalent ligand, these distances are shortened to about 2.0 Å for both of these interactions.

An additional prediction is that the terminal glycerol -OH can form a polar interaction with His269, which forms, along with Arg57 and Tyr194 the polar residues of the CA channel via which glycerol molecules (or other leaving groups) exit the protein. The CF_3 moiety does not appear to contribute to any favorable binding interactions. Rather, we believe its primary contribution to MAGL activity is manifest in the reactivity component, via the inductive effect of electronegative fluorines on the C=O bond.

The other half of the "pre-covalent" ligand occupies a space in the ACB pocket which is similar in orientation, but twisted about 60 degrees relative to the covalent ligand. Due to the change in position of Ser122, it is not possible to fit the carbonyl effectively in the oxyanion hole, while simultaneously preserving the exact position of the 'core' piece of the molecule to that of the covalent x-ray. It is our hypothesis that active MAGL ligands must be able to

effectively fit into multiple conformations in the ACB area in order to not hinder this rotation as the reaction proceeds. That the ACB pocket is lined with predominately hydrophobic residues (6 Leucine residues, 1 each Met, Phe and Ile) likely reflects the need for this pocket to favor non-specific binding, thus keeping energy wells for twisting shallow. This is further supported by the assortment of X-ray structures which show that a variety of binding poses can be accommodated.

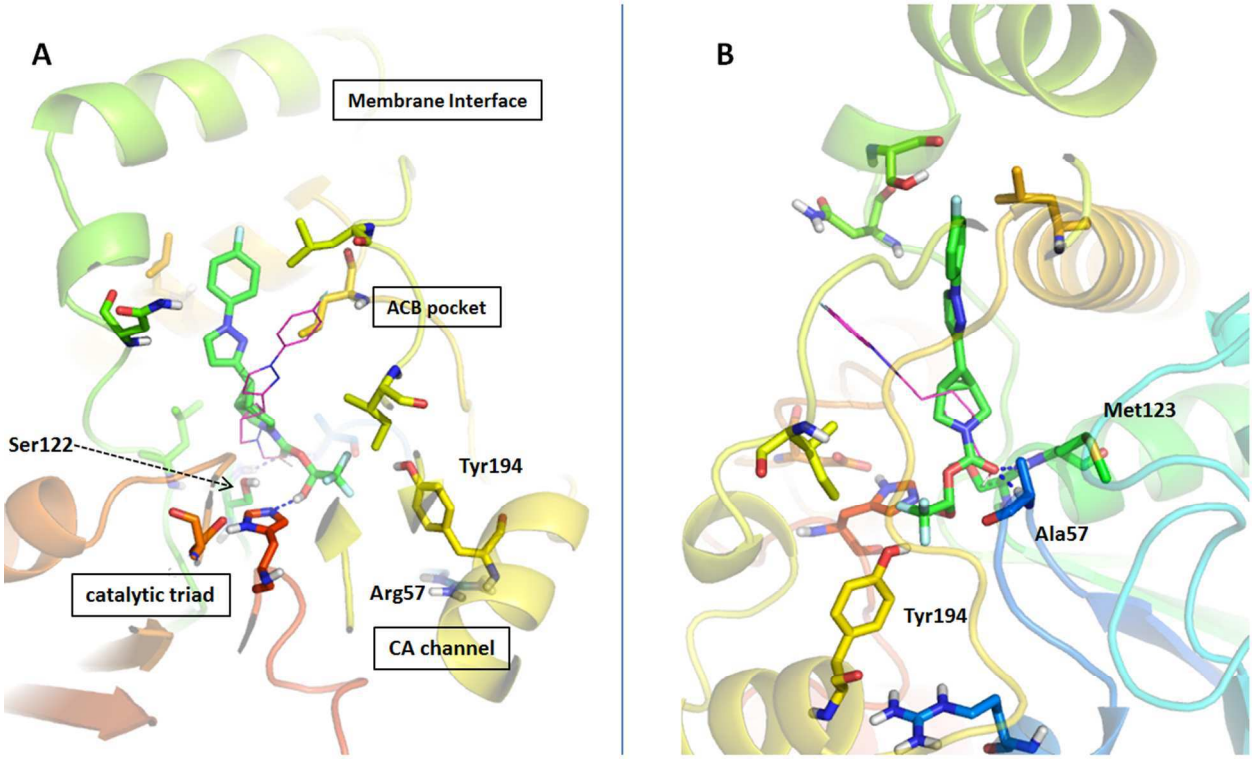

Figure 7. Docking model of compound **15** binding to MAGL in the pre-covalent state (green sticks). A superimposed X-ray structure of the post-covalent modification state is shown (purple lines- PDB Accession code: 6BQ0) (a) Shows predicted interaction of the leaving group "OH" with His239 of the catalytic triad. (b) Rotated view shows the predicted interaction of carbonyl group with backbone "NH" groups from Ala57 and Met123.

In vitro selectivity and in vitro safety profile. Serine hydrolase selectivity of compound **15** was tested in an *in vitro* panel of selected serine hydrolases (Figure 8).[53] Compound **15** exhibits

a comparably clean selectivity profile compared to analogs containing previously described leaving groups, such as HFIP (compound **8**) and NHS (compound **10**) analogs. Compound **15** shows complete inhibition of MAGL without significant inhibition of other serine hydrolases, with the exception of carboxyesterase 1(CES1), which is inhibited at 80% when tested at 10 μM. In contrast, HFIP analog **8** shows complete inhibition of MAGL, but also ABHD6 (95%) and CES1 (58%) at the same dose. NHS carbamate analog **10** had weaker off-target activity at a number of serine hydrolases, including the carboxyesterase enzymes (CES1 and CES2), ABHD6, FAAH and FAAH2.

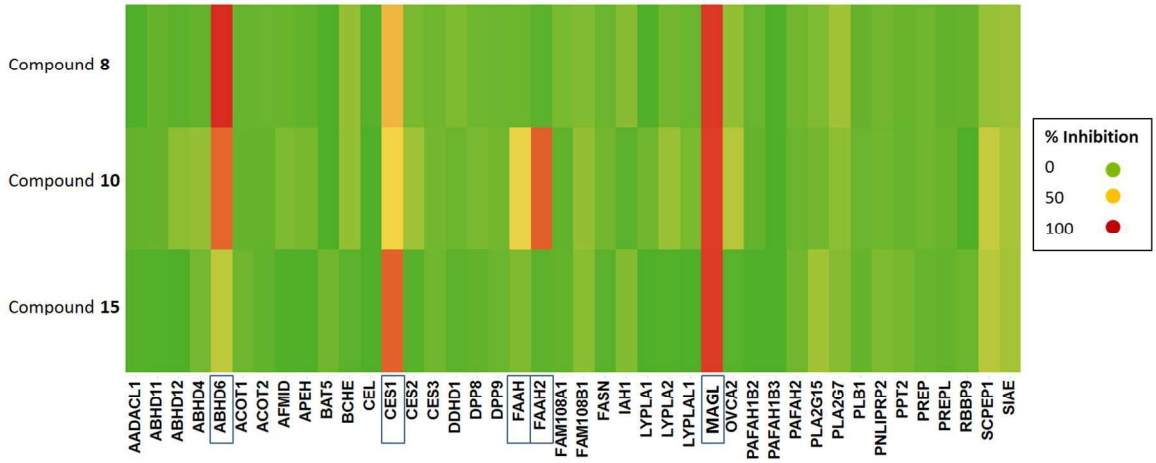

Figure 8. Heat map showing serine hydrolase inhibition profile for MAGL inhibitors dosed at 10μM against a panel of 42 human serine hydrolase enzymes (% Inhibition). A full list of serine hydrolase enzymes tested and method is provided in SI, table S2.

Compound **15** was also profiled for general off-target pharmacology in a binding/functional panel comprising a number of enzymes, transporters, receptors, and ion channel targets (CEREP). At a concentration of 10 μM, compound **15** hit only a single target, showing functional activity at the cannabinoid 1 receptor (EC_{50} = 1.5 μM). Follow up radioligand binding studies demonstrated a lack of activity at CB1, suggesting that the compound does not engage CB1 directly. An indirect functional CB1 agonism effect would be expected for a MAGL inhibitor due to the expected increase in 2-AG (a CB1 agonist). In addition, absence of binding at the hERG channel (IC_{50} >30 μM), also suggests a low risk of cardiovascular QT prolongation, further increasing the confidence in the safety profile of compound **15**.

In vitro metabolism and pharmacokinetic properties of compound 15. With the desired *in vitro* pharmacology and safety profile for compound **15**, the *in vitro* ADME properties were evaluated to assess suitability for *in vivo* studies (Table 3). *In vitro* screening data indicated high passive permeability, as measured by apparent passive permeability (P_{app}) in the Madin-Darby canine kidney low efflux cell line (MDCKII-LE; RRCK cell permeability assay = 21 x 10^{-6} cm/s). In addition, compound **15** was assessed for efflux via human P-glycoprotein (MDCKII-LE transfected with human MDR1) and mouse breast cancer-resistant protein (MDCKII-LE tranfected with mBCRP) using well-established transwell assay procedures.[54] The transporter efflux ratios were in the low range indicating minimal interaction with either transporter; increasing the probability of achieving sufficient brain penetration.

Compound **15** was evaluated in human *in vitro* clearance screening assays, including human liver microsomes and cryopreserved human hepatocytes (HHEPs) monitoring for substrate depletion.[55] In human liver microsomes (HLM), turnover of the compound was not observed

(HLM scaled Cl_{int} < 8 mL/min/kg); however, in HHEPs the turnover observed was significantly higher (HHEPs scaled Cl_{int} = 52 mL/min/kg). Taken together, the data suggested that cytochrome P450 (CYP)-mediated oxidative clearance was minimal with substantial involvement of a non-CYP-mediated clearance pathway. The hydroxyl group in compound **15** is a potential site for direct conjugation by enzymes such as uridine 5'-diphospho-glucuronosyltransferase (UGT) and/or sulfotransferase (SULT). To further explore the clearance pathways, compound **15** was incubated in HHEPs in the presence of aminobenzotriazole (ABT) and tienilic acid which result in pan-CYP inhibition. In the presence of the CYP inhibitors the turnover of compound **15** was only partially inhibited as compared with the control incubation without CYP inhibitors, indicating that the predominant clearance metabolism was non-CYP mediated with a minor oxidative component. The biotransformation of compound **15** was performed using HHEPs and the major metabolite identified was a direct glucuronide conjugate, supporting the hypothesis that compound **15** is cleared predominantly through direct glucuronidation on the hydroxyl of the leaving group. Compound **15** was also evaluated for competitive inhibition of five CYP enzymes (CYP3A4, 2D6, 2C9, 2C8, and 1A2) in screening assays using relevant probe substrates. The observed CYP inhibition was < 10% at 3 μM for each of the isoforms, indicating a low risk for drug-drug interactions mediated through competitive inhibition.

Table 3. Summary of chemical properties and *in vitro* ADME characteristics of compound **15**

Chemical Properties	
MW	399
PSA	68
eLogD	3.8
cLogP	2.7
Thermodynamic solubility pH 6.5 (μM)	25

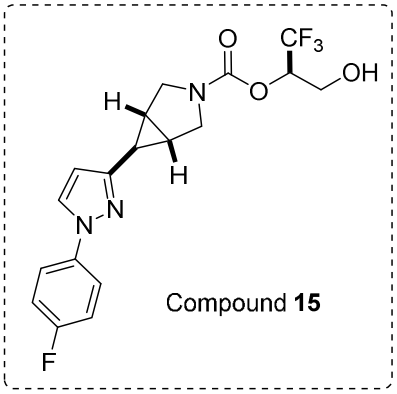

Compound **15**

In vitro ADME	
RRCK P_{app} (x 10^{-6} cm/s)[a]	21
MDR1 efflux ratio[b]	1.2
mBCRP efflux ratio[c]	1.3
HLM $CL_{int,scaled}$ (mL/min/kg)[d]	<8
HHEP $CL_{int,scaled}$ (mL/min/kg)[e]	52
HHEP $CL_{int,scaled}$ (mL/min/kg)(+ABT)[f]	37

[a]Permeability in the MDCKII-LE cell line. [b]Ratio of permeability, measured as a rate in 1 x10^{-6} cm/sec in and out (BA/AB) in the MDCKII-LE cell line transfected with MDR1 (human P-glycoprotein). [c]Ratio of permeability, measured as a rate in 1 x 10^{-6} cm/sec in and out (BA/AB) in the MDCKII-LE cell line transfected with mouse BCRP. [d]Scaled intrinsic clearance in human liver microsomes. [e]Scaled intrinsic clearance in human hepatocytes. [f]Scaled intrinsic clearance in human hepatocytes in the presence of CYP inhibitors. PSA = polar surface area

With an intriguing in vitro profile, in vivo pharmacokinetic (PK) properties were assessed. As we were targeting an intravenous therapy, IV PK studies in rat, dog, and non-human primate (nhp) were conducted (Table 4). Following IV administration, compound **15** exhibited a moderate to high plasma clearance (CL_p) and a moderate volume of distribution (V_d) cross-species. The resulting half-life was short, ranging from ~1-2 h, although sufficient for *in vivo* evaluation. Compound **15** was dosed subcutaneously to mice followed by collection of plasma and brain samples in a time course manner (Table 4). No impairment to brain penetration was observed, as evidenced by the $AUC_{(0\text{-}Tlast)}$-derived unbound brain to unbound plasma ratio ($C_{b,u}/C_{p,u}$) of ~1.4. We therefore concluded that compound **15** had an adequate PK profile to test central MAGL inhibition efficacy *in vivo*.

Table 4. In vivo pharmacokinetics of compound **15**

Species[a]	Administration Route[b]	CL_p (mL/min/kg)[c]	V_d (L/kg)	$T_{1/2}$ (h)	C_b/C_p[d]	$C_{b,u}/C_{pu}$[e]
rat	IV	61	3.1	1.3	nd	nd
dog	IV	21	1.6	1.7	nd	nd
nhp	IV	16	1.5	1.7	nd	nd
mouse	SC	nd	nd	nd	2.4	1.4

[a]Rat, dog, and nhp studies conducted at 1 mg/kg (n = 2 per species), mouse study conducted at 1.0 mg/kg. [b]IV = intravenous, SC = subcutaneous. [c]Plasma clearance. [d]$AUC_{(0\text{-}Tlast)}$-derived ratio of the drug concentration in mouse brain to the drug concentration in plasma. [e]$AUC_{(0\text{-}Tlast)}$-derived ratio of the unbound drug concentration in mouse brain to the unbound drug concentration in plasma (mouse fraction unbound in plasma, $f_{u,p}$ = 0.0135; mouse fraction unbound in brain, $f_{u,b}$ = 0.00775). nd = not determined.

In vivo PK/PD and Efficacy of compound 15. Compound **15** was tested in a wild type mouse PK/PD model to understand the relationship between 2-AG and AA changes with compound exposure in the brain. Mice (male C57Bl6) were administered a 1 mg/kg subcutaneous dose of compound **15**, and then brain levels of 2-AG and arachidonic acid were monitored over a 24 h time course. We observed the expected increase in brain 2-AG levels, which persisted for 8 h post dose, compared to vehicle treated mice (Figure 9a). In addition, a concomitant decrease in brain arachidonic acid level was observed compared to vehicle treated mice over a similar time period (Figure 9b). Excellent total brain exposure of compound **15** was achieved, with greater than one micromolar concentration at C_{max} (Figure 9c). Unbound brain concentrations of compound **15** above the IC_{50} (3 nM) were achieved (Figure 9d) until approximately 2 hours post-dose. Gratifyingly, as is expected from a covalent inhibitor, the desired PD response was observed for several hours beyond the PK time course.

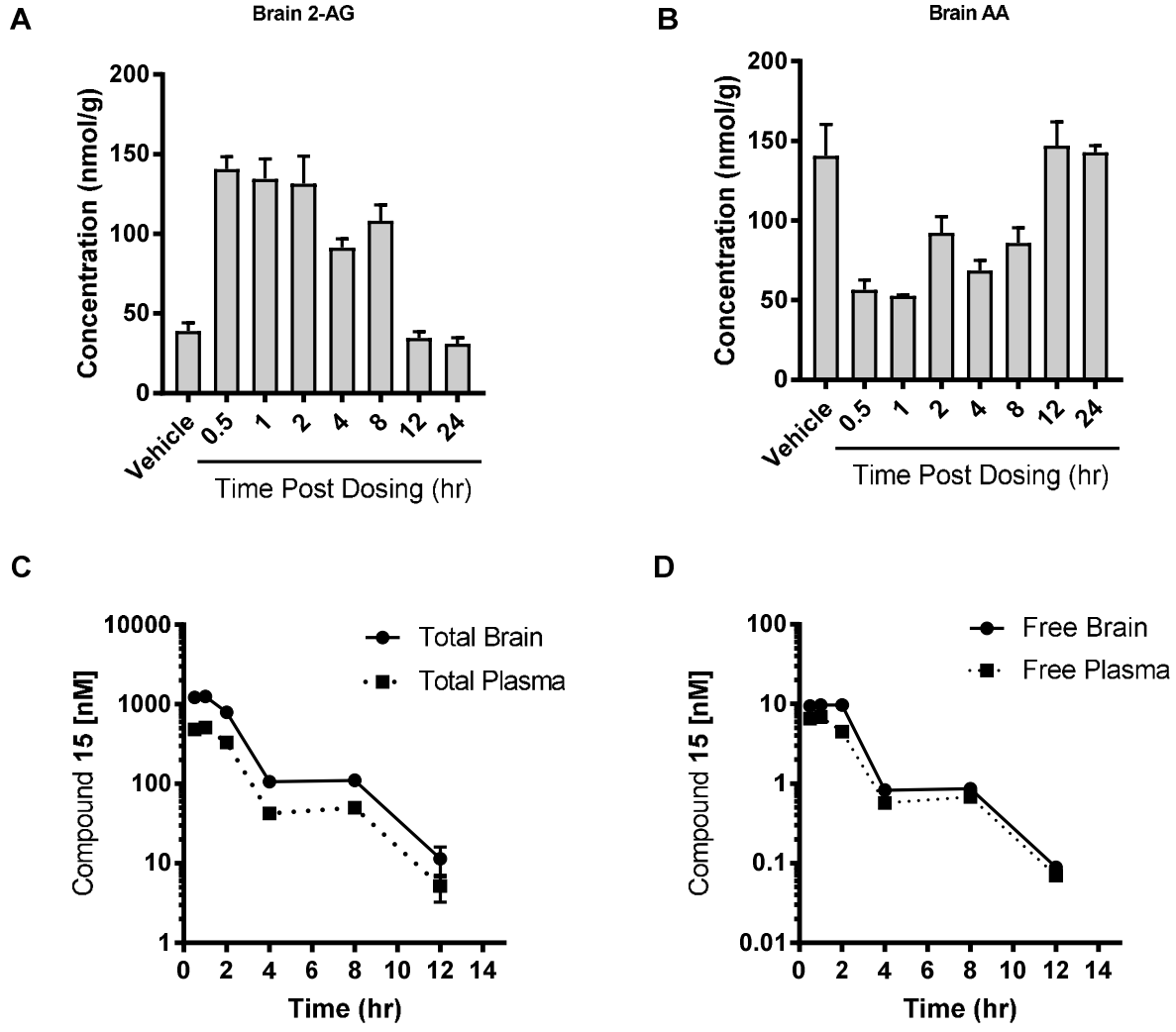

Figure 9 Effect of compound **15** following subcutaneous administration of a 1 mg/kg dose in mice. (a) brain 2-AG levels (b) brain AA levels (c) Total plasma and brain concentrations of compound **15** (d) Free plasma and brain concentrations of compound **15**.

Additionally, the effect of compound **15** in reducing brain levels of inflammatory mediators was tested in a mouse model of inflammation (Figure 10). A high dose of systemic lipopolysaccharide (LPS) was used to induce a sepsis or encephalitis-like state. As expected, 2-AG and AA levels were not impacted by LPS challenge, however, increases in brain PGE2, IL-

1β and TNF-α levels were observed, consistent with a central inflammatory response. Compound **15** was administered 30 minutes following the LPS dose, and then brain levels of 2-AG, AA, PGE2, IL-1β and TNF-α were measured at 4 hours post-challenge. Compound **15** was effective in significantly reducing levels of brain inflammatory markers relative to treatment with vehicle.

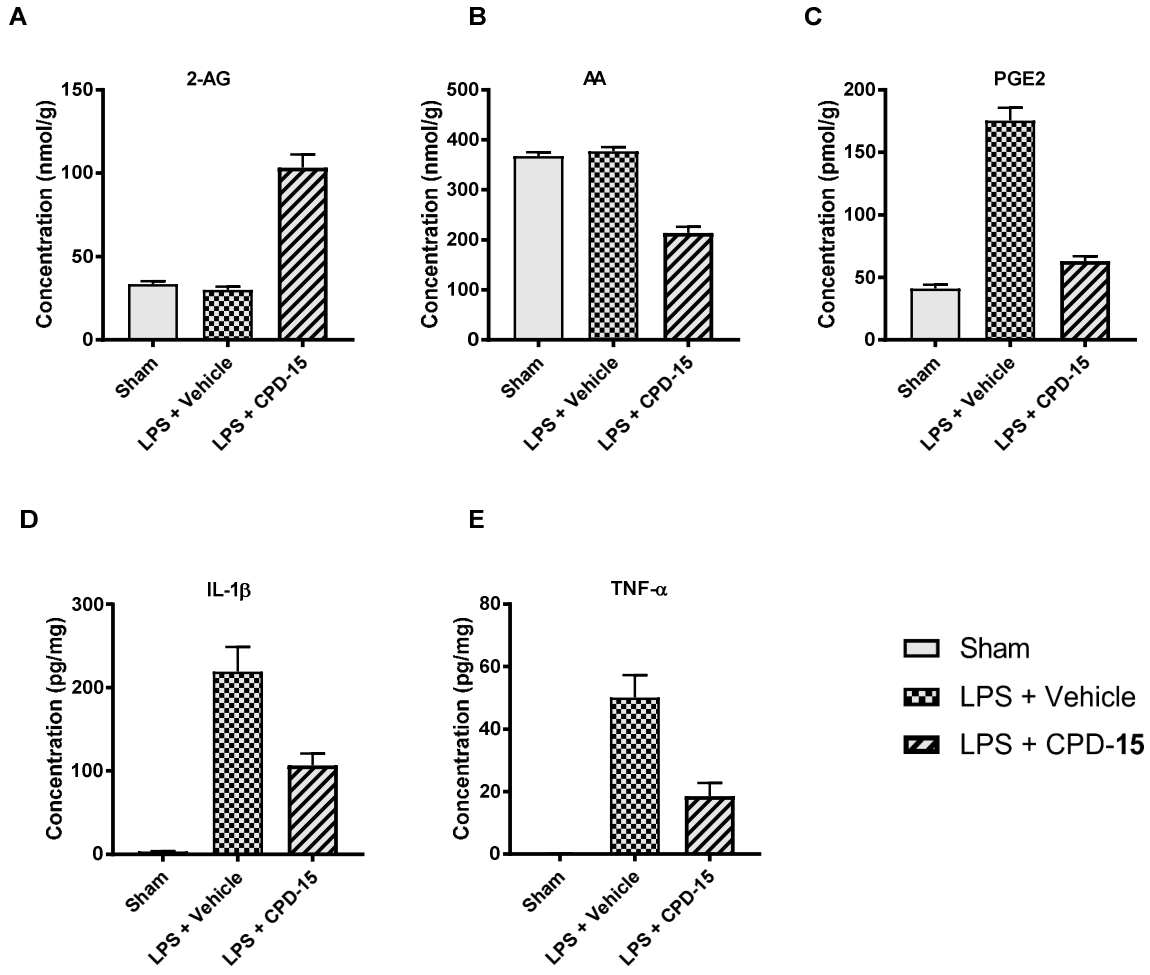

Figure 10. Effect of 1mg/kg of compound **15** dosed subcutaneously in mice 30 minutes following LPS challenge (20mg/kg dose, ip administration). **(a-e)** Brain levels of 2-AG, AA, and inflammatory markers measured 4 hours following LPS challenge

Conclusion

MAGL inhibition offers a compelling approach to the treatment of neuroinflammation and related diseases; this dictates the need for a potent, selective, brain penetrant MAGL inhibitor in favorable property space. A promising series of MAGL inhibitors based on a [3.1.0] pyrazole core system was identified, however, early leads from this series based on the HFIP leaving group resulted in highly lipophilic, low solubility compounds. Focused SAR efforts to identify a new leaving group with a desirable MAGL inhibition profile in improved physicochemical property space led to the identification of a unique trifluoromethylglycol leaving group. Combination with the optimized core system resulted in compound **15,** which has an excellent MAGL pharmacology profile, along with significantly improved physicochemical properties and LipE. The higher pKa of the trifluoromethyl glycol leaving group as compared with literature covalent MAGL inhibitor leaving groups confers a lower inherent chemical reactivity, and a lower propensity for non-specific reactivity is expected. Importantly, compound **15** shows significant solubility improvements as compared with analogs with a similar profile, furthering our objective in identifying MAGL inhibitors with a property profile amenable to IV dosing. Compound **15** also exhibits excellent serine hydrolase selectivity, and a clean *in vitro* safety profile. In addition, compound **15** showed good CNS exposure in mouse, and a suitable PK profile for use as a tool to explore *in vivo* efficacy. The expected elevation of mouse brain 2-AG was observed upon treatment with compound **15**, demonstrating target engagement *in vivo*. In addition, reductions in inflammatory mediators in the CNS were also observed following LPS challenge. Covalent MAGL inhibitors from this glycol leaving group series represent a significant advancement in the search for inhibitors that could be used as treatment for acute neuro inflammatory conditions with IV delivery.

EXPERIMENTAL

Chemistry

General Methods Solvents and reagents were of reagent grade and were used as supplied by the manufacturer. All reactions were run under a N_2 atmosphere. Organic extracts were routinely dried over anhydrous sodium sulfate. Concentration refers to rotary evaporation under reduced pressure. Chromatography refers to flash chromatography using disposable RediSepRf 4 to 120 g silica columns or Biotage disposable columns on a CombiFlash Companion or Biotage Horizon automatic purification system. Microwave reactions were carried out in a SmithCreator microwave reactor from Personal Chemistry. Purification by mass-triggered HPLC was carried out using Waters XTerra PrepMS C18 columns, 5μm, 30 x 100 mm. Compounds were pre-salted as TFA salts and diluted with 1 mL dimethylsulfoxide. Samples were purified by mass triggered collection using a mobile phase of 0.1% trifluoroacetic acid in water and acetonitrile with a starting gradient of 100% aqueous to 100% acetonitrile over 10 minutes at a flow rate of 20 mL/minute. Elemental analyses were performed by QTI, Whitehouse, NJ. All target compounds were analyzed using ultra high performance liquid chromatography /ultra violet/ evaporative light scattering detection coupled to time of flight mass spectrometry (UHPLC/UV/ELSD/TOFMS). All test compounds were found to be > 95% pure by this method.

UHPLC/MS Analysis. The UHPLC was performed on a Waters ACQUITY UHPLC system (Waters, Milford, MA), which was equipped with a binary solvent delivery manager, column manager, and sample manager coupled to ELSD and UV detectors (Waters, Milford, MA). Detection was performed on a Waters LCT premier XE mass spectrometry (Waters, Milford,

MA). The instrument was fitted with an Acquity BEH (Bridged Ethane Hybrid) C18 column (30 mm × 2.1 mm, 1.7 μm particle size, Waters, Milford, MA) operated at 60 ° C.

1,1,1,3,3,3-Hexafluoropropan-2-yl 3-(1-(4-fluorophenyl)-*1H*-pyrazol-3-yl)azetidine-1-carboxylate (7)

A mixture of *tert*-butyl 3-(*1H*-pyrazol-3-yl)azetidine-1-carboxylate (20 g, 90 mmol), 4-fluorophenyl boronic acid [45] (13.8 g, 98.5 mmol), $Cu(OAc)_2$ (24.4 g, 13 mmol), pyridine (14.2 g, 18 mmol), and 4 Å molecular sieves (2.5 g) in CH_2Cl_2 (800 mL) was stirred at room temperature for 48 h. The reaction mixture was then filtered and the filtrate was diluted with water (20 mL) and extracted with CH_2Cl_2 (500 mL x 3). The combined organic layer was washed with water (500 mL) and saturated sodium chloride (500 mL), dried over sodium sulfate, concentrated in vacuo and purified by silica gel chromatography (ethyl acetate/petroleum ether) to give 20 g (71%) of solid *tert*-butyl 3-[1-(4-fluorophenyl)-*1H*-pyrazol-3-yl]azetidine-1-carboxylate. ^{1}H NMR (400 MHz, $CDCl_3$) δ ppm 7.81 (d, J=2.3 Hz, 1 H), 7.68 - 7.55 (m, 2 H), 7.18 - 7.06 (m, 2 H), 6.42 (d, J=2.7 Hz, 1 H), 4.32 (dd, J=8.9, 8.4 Hz, 2 H), 4.10 (dd, J=8.4, 6.0 Hz, 2 H), 3.87 (tt, J=8.9, 6.0 Hz, 1 H), 1.46 (s, 9H). ^{13}C NMR (101 MHz, $CDCl_3$) δ 161.0 (d, J=245.8 Hz), 156.4, 155.0, 136.4 (d, J=2.9 Hz), 128.0, 120.7 (d, J=8.1 Hz), 116.1 (d, J=23.5 Hz), 105.3, 79.4, 55.3 (br s, 2C), 28.4, 27.5.

To a solution of *tert*-butyl 3-[1-(4-fluorophenyl)-*1H*-pyrazol-3-yl]azetidine-1-carboxylate (80 mg, 0.25 mmol) in CH_2Cl_2 (4 mL) was added TFA (1 mL). The resulting mixture was stirred at 25 °C for 2 h. The reaction was concentrated in vacuo to afford 120 mg of crude 3-(azetidin-3-yl)-1-(4-fluorophenyl)-*1H*-pyrazole trifluoroacetate salt. LCMS *m/z* 217.7 [M + H]+.

Bis(pentafluorophenyl)carbonate (235 mg, 1.4 mmol) and trimethylamine (708 mg, 6.99 mmol) were added to a solution of 2,2,2-trifluoroethanol (235 mg, 1.4 mmol) in 8 mL of

acetonitrile at 0 °C. The solution was warmed to room temperature over 1 h. An aliquot of the above solution (3.5 mL) was added to a solution of crude 3-(azetidin-3-yl)-1-(4-fluorophenyl)-*1H*-pyrazole trifluoroacetate salt (55 mg, 0.25 mmol) in 2 mL of acetonitrile. The resulting solution was stirred at room temperature for 16 h. The mixture was concentrated and purified by preparative reverse phase HPLC to afford 51 mg of **7** (1,1,1,3,3,3-hexafluoropropan-2-yl 3-(1-(4-fluorophenyl)-*1H*-pyrazol-3-yl)azetidine-1-carboxylate). ^{1}H NMR (400 MHz, $CDCl_3$) δ ppm 7.85 (d, J=2.4 Hz, 1 H), 7.70 - 7.58 (m, 2 H), 7.21 - 7.11 (m, 2 H), 6.42 (d, J=2.4 Hz, 1 H), 5.73 – 5.67 (m, 1 H), 4.55 – 4.47 (m, 2 H), 4.39 - 4.25 (m, 2 H), 4.10 - 3.97 (m, 1 H). LCMS *m/z* 412.0 [M + H]+.

1,1,1,3,3,3-Hexafluoropropan-2-yl (*1R,5S,6r*)-6-[1-(4-fluorophenyl)-*1H*-pyrazol-3-yl]-3-azabicyclo[3.1.0]hexane-3-carboxylate (8). To a solution of 1,1,1,3,3,3-hexafluoropropan-2-ol (257 mg, 1.53 mmol) and trimethylamine (774 mg, 7.65 mmol) in anhydrous acetonitrile (6 mL) at 0 ^{o}C was added dipentafluorophenyl carbonate (603 mg, 1.53 mmol). The solution was stirred at 0 °C for 30 minutes, warmed to 10 °C, and stirred at 10 °C for 2 h. A solution of (*1R,5S,6r*)-6-[1-(4-fluorophenyl)-*1H*-pyrazol-3-yl]-3-azabicyclo[3.1.0]hexane, trifluoroacetate salt (**24**) (364 mg, 1.02 mmol) and trimethylamine (515 mg, 5.09 mmol) in 5 mL of acetonitrile was added and the resulting mixture was stirred at 10 °C for 16 h. The reaction was concentrated *in vacuo* and purified by preparative reverse phase HPLC to afford 253 mg (57%) of **8** as a white solid. ^{1}H NMR (400 MHz, $CDCl_3$) δ ppm 7.75 (d, *J*=2.4 Hz, 1 H), 7.64-7.56 (m, 2 H), 7.17-7.09 (m, 2 H), 6.20 (d, *J*=2.4 Hz, 1 H), 5.74 (sep, *J*=6.3 Hz, 1 H), 3.88 (dd, *J*=11.1, 2.7 Hz, 2 H), 3.67 (dd, *J*=11.1, 3.9 Hz, 2 H), 2.08 - 2.06 (m, 2 H), 1.87 (t, *J*=3.4 Hz, 1 H). ^{13}C NMR (101 MHz, $CDCl_3$) δ 160.0 (d, *J*=245.0 Hz), 153.1, 151.2, 136.4 (d, *J*=2.9 Hz), 127.5, 120.6 (d, *J*=8.1 Hz), 116.2 (d,

J=22.7 Hz), 105.2, 67.8 (sep, *J*=34.5 Hz), 49.7, 48.8, 25.8, 25.1, 21.2, CF_3 carbons not observed. HRMS (ESI) *m/z* calculated for $C_{18}H_{14}F_7N_3O_2$ [M + H+]: 438.1047. Found 438.1058.

4-Nitrophenyl (*1R,5S,6r*)-6-[1-(4-fluorophenyl)-*1H*-pyrazol-3-yl]-3-azabicyclo[3.1.0]hexane-3-carboxylate (9). To a solution of (*1R,5S,6r*)-6-[1-(4-fluorophenyl)-*1H*-pyrazol-3-yl]-3-azabicyclo[3.1.0]hexane, trifluoroacetate salt (**24**) (82 mg, 0.17 mmol) and trimethylamine (88 mg, 0.87 mmol) in dichloromethane was added 4-nitrophenyl chloroformate (110 mg, 0.56 mmol). The mixture was stirred at 30 °C for 27 h and concentrated under reduced pressure. The resulting residue was purified by reverse phase preparative HPLC to afford 3.8 mg (5%) of **9** as a white solid. ^{1}H NMR (400 MHz, $CDCl_3$) δ ppm 8.27 (d, *J*=9.0 Hz, 2 H), 7.76 (d, *J*=2.5 Hz, 1 H), 7.64-7.57 (m, 2 H), 7.34 (d, *J*=9.0 Hz, 2 H), 7.18 - 7.11 (m, 2 H), 6.22 (d, *J*=2.5 Hz, 1 H), 4.01 (d, *J*=11.0 Hz, 1 H), 3.93 (d, *J*=11.0 Hz, 1 H), 3.78 (dd, *J*=11.0, 3.0 Hz, 1 H), 3.69 (dd, *J*=11.0, 3.5 Hz, 1 H), 2.13-2.07 (m, 2 H), 1.96 (t, *J*=3.5 Hz, 1 H). LCMS *m/z* 408.9 $[M+H]^+$.

1-[({(*1R,5S,6r*)-6-[1-(4-Fluorophenyl)-*1H*-pyrazol-3-yl]-3-azabicyclo[3.1.0]hex-3-yl}carbonyl)oxy]pyrrolidine-2,5-dione (10). A solution of N-hydroxysuccinimide (19 mg, 0.17 mmol), 4-dimethylaminopyridine (2 mg, 0.017 mmol), and *N,N*-diisopropylethylamine (26 mg, 0.20 mmol) in 5 mL of methylene chloride was added dropwise at 0 °C to a solution of triphosgene (16 mg, 0.56 mmol) in 3 mL of methylene chloride. The resulting mixture was stirred at room temperature for 16 h and subsequently added dropwise to a solution of (*1R,5S,6r*)-6-[1-(4-fluorophenyl)-*1H*-pyrazol-3-yl]-3-azabicyclo[3.1.0]hexane, trifluoroacetate salt (**24**) (60 mg, 0.17 mmol) and *N,N*-diisopropylethylamine (87 mg, 0.67 mmol) in 2 mL of dichloromethane. The mixture was stirred at room temperature for an additional 16 h, diluted

with water (30 mL), and extracted with methylene chloride (3 x 30 mL). The combined organic extracts were washed with water and brine, dried (Na_2SO_4), filtered, and concentrated at reduced pressure. The crude residue obtained was purified by reverse phase preparative HPLC to afford 51 mg (79%) of **10**. ^{1}H NMR (400 MHz, $CDCl_3$) δ ppm 7.74 (d, *J*=2.3 Hz, 1 H), 7.64-7.55 (m, 2 H), 7.13 (dd, *J*=8.6, 8.6 Hz, 2 H), 6.23 (d, *J*=2.3 Hz, 1 H), 3.99 (d, *J*=10.9 Hz, 1 H), 3.87 (d, *J*=10.9 Hz, 1 H), 3.78 (dd, *J*=10.9, 3.9 Hz, 1 H), 3.69 (dd, *J*=10.9, 3.9 Hz, 1 H), 2.83 (s, 4 H), 2.16-2.05 (m, 2 H), 1.95 (t, *J*=3.9 Hz, 1 H). ^{13}C NMR (101 MHz, $CDCl_3$) δ 169.7 (2C), 160.9 (d, *J*=245.0 Hz), 153.1, 150.1, 136.4 (d, *J*=2.9 Hz), 127.4, 120.5 (d, *J*=8.1 Hz), 116.1 (d, *J*=23.5 Hz), 105.5, 50.2, 48.8, 26.2, 25.5 (2C), 24.9, 21.1. LCMS *m/z* 385.1 $[M+H]^+$.

1,1,1-Trifluoropropan-2-yl (*1R,5S,6r*)-6-[1-(4-fluorophenyl)-*1H*-pyrazol-3-yl]-3-azabicyclo[3.1.0]hexane-3-carboxylate (11). Bis(pentafluorophenyl)carbonate (59 mg, 0.15 mmol) and trimethylamine (75 mg, 0.75 mmol) were added to a solution of 1,1,1-trifluoro-2-propanol (17 mg, 0.15 mmol) in 1 mL of acetonitrile at 0 °C. The solution was warmed to 20 °C and stirred at that temperature for 1 h. A solution of (*1R,5S,6r*)-6-[1-(4-fluorophenyl)-*1H*-pyrazol-3-yl]-3-azabicyclo[3.1.0]hexane, trifluoroacetate salt (**24**) (50 mg, 0.11 mmol) and triethylamine (54 mg, 0.53 mmol) in 3 mL of acetonitrile was added and the mixture was stirred at 20 °C for 16 h. The solution was concentrated and purified by preparative TLC (20% EtOAc in petroleum ether) to afford 35 mg of impure product. The product was further purified by reverse phase preparative HPLC to afford 17 mg (41%) of **11** as a white solid. By ^{1}H NMR analysis, this was judged to be a mixture of rotamers. ^{1}H NMR (400 MHz, $CDCl_3$) δ ppm 7.74 (br s, 1 H), 7.63-7.56 (m, 2 H), 7.15-7.11 (m, 2 H), 6.20 (d, *J*= 2.5 Hz, 0.5 H), 6.17 (d, *J*= 2.5 Hz, 0.5 H), 5.30-5.21 (m, 2 H), 3.84-3.78 (m, 2 H), 3.63-3.54 (m, 2 H), 2.05-1.99 (m, 2 H), 1.88-1.83 (m, 1 H), 1.42 (d, *J*=6.5 Hz, 3 H). ^{13}C NMR (101 MHz, $CDCl_3$) δ 160.9 (d, *J*=245.8 Hz), 153.6,

153.5, 153.3, 136.4 (d, *J*=2.9 Hz), 127.5, 127.4, 124.2 (q, *J*=280.2Hz), 120.6 (d, *J*=8.1 Hz), 116.2 (d, *J*=22.7 Hz), 105.2, 105.0, 67.7 (q, *J*=33.0 Hz), 67.6 (q, *J*=33.0 Hz), 49.1, 49.0, 48.5, 48.4, 26.0, 25.21, 25.18, 21.1, 21.0, 14.0. LCMS *m/z* 383.9 $[M+H]^+$.

2,2,2-Trifluoroethyl (*1R,5S,6r*)-6-[1-(4-fluorophenyl)-*1H*-pyrazol-3-yl]-3-azabicyclo[3.1.0]hexane-3-carboxylate (12). Bis(pentafluorophenyl)carbonate (99 mg, 0.25 mmol) and trimethylamine (126 mg, 1.25 mmol) were added to a solution of 2,2,2-trifluoroethanol (25 mg, 0.25 mmol) in 2 mL of acetonitrile at 0 °C. The solution was stirred at 0 °C for 1 h. A solution of (*1R,5S,6r*)-6-[1-(4-fluorophenyl)-*1H*-pyrazol-3-yl]-3-azabicyclo[3.1.0]hexane, trifluoroacetate salt (**24**) (82 mg, 0.17 mmol) and triethylamine (88 mg, 0.87 mmol) in 2 mL of acetonitrile was added, and the mixture was stirred at 15 °C for 2 h. The solution was concentrated and purified by preparative TLC (20% EtOAc in petroleum ether) to afford 40 mg of impure product. The product was further purified by reverse phase preparative HPLC to afford 19 mg (30%) of **12** as a white solid. ^{1}H NMR (400 MHz, $CDCl_3$) δ ppm 7.74 (br s, 1 H), 7. 61-7.57 (m, 2 H), 7.15-7.10 (m, 2 H), 6.18 (br s, 1 H), 4.49 (q, *J*=8.5 Hz, 2 H), 3.84 (t, *J*=11.8 Hz, 2 H), 3.59 (br d, *J*=11.8 Hz, 2 H), 2.03 (br s, 2 H), 1.85 (br s, 1 H). ^{13}C NMR (101 MHz, $CDCl_3$) δ 160.9 (d, *J*=245.0 Hz), 153.5, 153.2, 136.4 (d, *J*=2.9 Hz), 127.5, 123.2 (q, *J*=278.0 Hz), 120.6 (d, *J*=8.1 Hz), 116.2 (d, *J*=22.7 Hz), 105.1, 61.2 (q, *J*=36.7 Hz), 49.2, 48.6, 26.0, 25.2, 21.1. LCMS *m/z* 369.8 $[M+H]^+$.

(2R)-1,1,1,3-Tetrafluoropropan-2-yl (*1R,5S,6r*))-6-[1-(4-fluorophenyl)-*1H*-pyrazol-3-yl]-3-azabicyclo[3.1.0]hexane-3-carboxylate (13). To a solution of (2R)-1,1,1-trifluoro-3-hydroxypropan-2-yl (*1R,5S,6r*)-6-[1-(4-fluorophenyl)-*1H*-pyrazol-3-yl]-3-azabicyclo[3.1.0]hexane-3-carboxylate (118 mg, 0.30 mmol) in 4 mL of methylene chloride at 0 °C was added *N,N*-diethylaminosulfur trifluoride (71 mg, 0.44 mmol). The mixture was stirred

at 10 °C for 2 h, quenched by the additional of saturated NH_4Cl, and extracted with methylene chloride (2 x 20 mL). The combined organic extracts were concentrated at reduced pressure and purified by reverse phase preparative HPLC to afford 40 mg (34%) of **13**. By ^1H and ^{13}C NMR analysis, the product was judged to be a mixture of rotamers. ^1H NMR (400 MHz, $CDCl_3$) δ ppm 7.74 (d, *J*=2.5 Hz, 1 H), 7.64-7.56 (m, 2 H), 7.13 (m, 2 H), 6.19 (br s, 1 H), 5.55-5.40 (m, 1 H), 4.80-4.58 (m, 2 H), 3.91 - 3.82 (m, 2 H), 3.68 - 3.58 (m, 2 H), 2.05 (br. s., 2 H), 1.89 - 1.85 (m, 1 H). ^{13}C NMR (101 MHz, $CDCl_3$)δ 160.9 (d, *J*=245.0 Hz), 153.4, 152.7, 136.4 (d, *J*=2.9 Hz), 127.5, 120.6 (d, *J*=8.1 Hz), 116.2 (d, *J*=23.5 Hz), 105.15, 105.12, 79.0 (br d, *J*=177.5 Hz), 69.4 (m), 49.4, 49.3, 48.7, 48.6, 21.97, 21.95, 25.16, 25.14, 21.16, 21.13, all carbons not observed. LCMS *m/z* 401.9 $[M+H]^+$.

1,1,1-Trifluoro-3-hydroxypropan-2-yl (*1R,5S,6r*)-6-[1-(4-fluorophenyl)-*1H*-pyrazol-3-yl]-3-azabicyclo[3.1.0]hexane-3-carboxylate (14).

To a solution of triphosgene (129 mg, 0.436 mmol) in DCM (10 mL) was added a solution of racemic 1,1,1-trifluoro-3-(4-methoxybenzyloxy)propan-2-ol (327 mg, 1.31 mmol), DMAP (10.6 mg, 0.09 mmol) and DIPEA (203 mg, 1.57 mmol) in DCM (15 mL) dropwise at -10 ^oC under N_2 over 3 h. The mixture was stirred overnight at room temperature. The solution of reaction mixture was added to a solution of (*1R,5S,6r*)-6-[1-(4-fluorophenyl)-*1H*-pyrazol-3-yl]-3-azabicyclo[3.1.0]hexane, trifluoroacetate salt (**24**) (212 mg, 0.87 mmol) in DCM (10 mL) at room temperature. The mixture was stirred for 5 h at room temperature. The mixture was washed with water (20 mL). The aqueous layer was extracted with EtOAc (20 mL x 3). The combined organic layers were concentrated in vacuo and the crude residue obtained was purified by flash chromatography (0-50% EtOAc in petroleum ether) to give

1,1,1-trifluoro-3-[(4-methoxybenzyl)oxy]propan-2-yl (*1R,5S,6r*)-6-[1-(4-fluorophenyl)-*1H*-pyrazol-3-yl]-3-azabicyclo[3.1.0]hexane-3-carboxylate (340 mg, around 45% purity (W/W) from NMR). The product from the reaction was used in the next step without additional purification.

To a solution of crude 1,1,1-trifluoro-3-[(4-methoxybenzyl)oxy]propan-2-yl (*1R,5S,6r*)-6-[1-(4-fluorophenyl)-*1H*-pyrazol-3-yl]-3-azabicyclo[3.1.0]hexane-3-carboxylate (340 mg) in EtOH (100 mL) was added dry Pd/C (1500 mg, 10% w/w) under Ar. The mixture was charged with H_2, and the mixture was stirred for 3h under H_2 (40 psi) at room temperature. The mixture was filtered. The filtrate was concentrated in vacuo, and the crude residue obtained was purified by preparative TLC (petroleum ether: EtOAc = 2:1) to give 30 mg (9% over 2 steps) of (1,1,1-Trifluoro-3-hydroxypropan-2-yl (*1R,5S,6r*)-6-[1-(4-fluorophenyl)-*1H*-pyrazol-3-yl]-3-azabicyclo[3.1.0]hexane-3-carboxylate (**14**) as a white solid. ^{1}H NMR (400 MHz, $CDCl_3$) δ ppm 7.75 (d, *J*=2.0 Hz, 1 H), 7.59 (dd, *J*=9.0, 4.5 Hz, 2 H), 7.13 (dd, *J*=9.0, 8.5 Hz, 2 H), 6.19 (br. s., 1 H), 5.33 - 5.19 (m, 1 H), 4.05 – 3.97 (m, 1 H), 3.94 - 3.80 (m, 3 H), 3.69 - 3.57 (m, 2 H), 2.35 – 2.28 (m, 1 H), 2.05 (br. s., 2 H), 1.93 - 1.83 (m, 1 H). LCMS *m/z* 399.8 [M + H]+

(2R)-1,1,1-Trifluoro-3-hydroxypropan-2-yl (*1R,5S,6r*)-6-[1-(4-fluorophenyl)-*1H*-pyrazol-3-yl]-3-azabicyclo[3.1.0]hexane-3-carboxylate (15). To a solution of (R)-1,1,1-trifluoro-3-(4-methoxybenzyloxy)propan-2-ol (701 mg, 2.80 mmol) in dichloromethane (20 mL) were added triethylamine (850 mg, 8.40 mmol) and 1,1'-[carbonylbis(oxy)]dipyrrolidine-2,5-dione (717 mg, 2.80 mmol). The reaction mixture was stirred for 18 h at 25 °C and was then treated with a solution of (*1R,5S,6r*)-6-[1-(4-fluorophenyl)-*1H*-pyrazol-3-yl]-3-azabicyclo[3.1.0]hexane, trifluoroacetate salt (**24**) (2.9 mmol) and triethylamine (566 mg, 5.59 mmol) in dichloromethane

(10 mL). The reaction mixture was stirred overnight at 18 °C, whereupon it was concentrated *in vacuo*. Purification using silica gel chromatography (Gradient: 0% to 25% ethyl acetate in petroleum ether) provided 900 mg (61%) of (2R)-1,1,1-trifluoro-3-[(4-methoxybenzyl)oxy]propan-2-yl (*1R,5S,6r*)-6-[1-(4-fluorophenyl)-*1H*-pyrazol-3-yl]-3-azabicyclo[3.1.0]hexane-3-carboxylate as a gum. By ^{1}H NMR analysis, this was judged to be a mixture of rotamers. ^{1}H NMR (400 MHz, $CDCl_3$) δ 7.74 (d, *J*=2.4 Hz, 1H), 7.62-7.57 (m, 2H), 7.29-7.24 (m, 2H), 7.13 (br dd, *J*=8.9, 8.3 Hz, 2H), 6.93-6.88 (m, 2H), 6.19 (d, *J*=2.4 Hz, 0.5H), 6.16 (d, *J*=2.4 Hz, 0.5H), 5.53-5.43 (m, 1H), 4.60-4.54 (m, 1H), 4.48 (d, half of AB quartet, *J*=11.7 Hz, 1H), 3.90-3.84 (m, 1H), 3.84-3.73 (m, 2H), 3.82 (s, 0.5 x 3H) and 3.79 (s, 0.5 x 3H), 3.73-3.65 (m, 1H), 3.65-3.54 (m, 2H), 2.04-2.00 (m, 2H), 1.87-1.82 (m, 1H). LCMS *m/z* 520.1 $[M+H]^+$.

Trifluoroacetic acid (10 mL) was added to a solution of (2R)-1,1,1-trifluoro-3-[(4-methoxybenzyl)oxy]propan-2-yl (*1R,5S,6r*)-6-[1-(4-fluorophenyl)-*1H*-pyrazol-3-yl]-3-azabicyclo[3.1.0]hexane-3-carboxylate (890 mg, 1.7 mmol) in dichloromethane (30 mL), and the reaction mixture was stirred for 4 h at 15 °C. It was then slowly poured into saturated aqueous sodium bicarbonate solution, and the resulting mixture was extracted with dichloromethane (3 x 50 mL). The combined organic layers were dried over sodium sulfate, filtered, and concentrated *in vacuo*. The crude residue obtained was purified by chromatography on silica gel (Gradient: 0% to 50% ethyl acetate in petroleum ether) to afford 440 mg (65%) of **15** as a white solid. By ^{1}H NMR analysis, this was judged to be a mixture of rotamers. ^{1}H NMR (400 MHz, $CDCl_3$) δ 7.74 (d, *J*=2.4 Hz, 1H), 7.63-7.56 (m, 2H), 7.13 (dd, *J*=8.7, 8.5 Hz, 2H), 6.21-6.17 (m, 1H), 5.31-5.21 (m, 1H), 4.06-3.96 (m, 1H), 3.93-3.80 (m, 3H), 3.67-3.58 (m, 2H), 2.38-2.27 (br m, 1H), 2.08-2.01 (m, 2H), 1.90-1.84 (m, 1H). ^{13}C NMR (101 MHz, $CDCl_3$) δ 160.9 (d, *J*=245.8

Hz), 153.72, 153.67, 153.39, 153.35, 136.42 (d, *J*=2.9 Hz), 136.39 (d, *J*=2.9 Hz), 127.53, 127.50, 120.6 (d, *J*=8.1 Hz), 116.2 (d, *J*=22.0 Hz), 105.2, 105.1, 72.6 (q, *J*=30.8 Hz), 72.5 (q, *J*=31.5 Hz), 60.3 (overlapping quartets, CH_2OH), 49.33, 49.28, 48.74, 48.65, 25.9, 25.17, 25.15, 24.14, 21.13, CF_3 carbon not observed. LCMS *m/z* 400.2 [M + H]+. HRMS (ESI) *m/z* calculated for $C_{18}H_{17}F_4N_3O_3$ [M + H+]: 400.1279. Found 400.1274.

(2S)-1,1,1-Trifluoro-3-hydroxypropan-2-yl (*1R,5S,6S*)-6-[1-(4-fluorophenyl)-1H-pyrazol-3-yl]-3-azabicyclo[3.1.0]hexane-3-carboxylate (16). Bis(pentafluorophenyl)carbonate (258 mg, 0.66 mmol) and trimethylamine (332 mg, 3.28 mmol) were added to a solution of (S)-1,1,1-trifluoro-3-(4-methoxybenzyloxy)propan-2-ol (164 mg, 0.66 mmol) in 2 mL of acetonitrile at 0 °C. The solution was warmed to 10 °C and stirred at that temperature for 2 h. A solution of (*1R,5S,6r*)-6-[1-(4-fluorophenyl)-*1H*-pyrazol-3-yl]-3-azabicyclo[3.1.0]hexane, trifluoroacetate salt (**24**) (156 mg, 0.44 mmol) and triethylamine (221 mg, 2.18 mmol) in 3 mL of acetonitrile was added and the mixture was stirred at 15 °C for 16 h. The solution was concentrated and purified by flash chromatography on silica gel (Gradient: 0% to 18% ethyl acetate in petroleum ether) to afford 200 mg (88%) of (2S)-1,1,1-trifluoro-3-hydroxypropan-2-yl (*1R,5S,6S*)-6-[1-(4-fluorophenyl)-*1H*-pyrazol-3-yl]-3-azabicyclo[3.1.0]hexane-3-carboxylate as a colorless gum. By ^{1}H NMR analysis, this was judged to be a mixture of rotamers. ^{1}H NMR (400 MHz, $CDCl_3$) δ ppm 7.74 (d, *J*=2.5 Hz, 1 H), 7.63-7.56 (m, 2 H), 7.30-7.24 (m, 2 H), 7.17-7.09 (m, 2 H), 6.94-6.87 (m, 2 H), 6.19 (d, *J*=2.5 Hz, 0.5 H), 6.17 (d, *J*=2.5 Hz, 0.5 H), 5.52-5.44 (m, 1 H), 4.57 (d, *J*=11.5 Hz, 0.5 H), 4.56 (d, *J*=11.5 Hz, 0.5 H) 4.48 (d, *J*=11.5 Hz, 1 H), 3.89-3.55 (m, 6 H), 3.82 (s, 0.5 x 3 H), 3.80 (s, 0.5 x 3 H), 2.04-2.00 (m, 2 H), 1.88-1.82 (m, 1 H). LCMS *m/z* 520.1 $[M+H]^+$.

Trifluoroacetic acid (1 mL) was added to a solution of (of (2S)-1,1,1-trifluoro-3-hydroxypropan-2-yl (*1R,5S,6S*)-6-[1-(4-fluorophenyl)-*1H*-pyrazol-3-yl]-3-azabicyclo[3.1.0]hexane-3-carboxylate (200 mg, 0.39 mmol) in dichloromethane (4 mL), and the reaction mixture was stirred for 1 h at 10 °C. The reaction mixture was concentrated, diluted with 30 mL of EtOAc, and washed with saturated $NaHCO_3$ (20 mL). The aqueous was further extracted with EtOAc (3 X 30 mL), and the combined organic extracts were dried (Na_2SO_4), filtered, and concentrated. The crude residue obtained was purified by reverse phase preparative HPLC to afford 97 mg (63%) of **16** as a white solid. By ^1H and ^{13}C NMR analysis, the product was judged to be a mixture of rotamers. ^1H NMR (400 MHz, $CDCl_3$) δ ppm 7.75 (d, *J*=2.4 Hz, 1 H), 7.63-7.56 (m, 2 H), 7.18-7.08 (m, 2 H), 6.23-6.16 (m, 1 H), 5.32-5.21 (m, 1 H), 4.01 (dd, *J*= 12.2, 2.9 Hz, 1 H), 3.94-3.81 (m, 3 H), 3.67-3.59 (m, 2 H), 2.08-2.01 (m, 2 H), 1.87 (m, 1 H). ^{13}C NMR (101 MHz, $CDCl_3$) δ 160.88 (d, *J*=245.8 Hz), 160.87 (d, *J*=245.0 Hz), 153.70, 153.69, 153.43, 153.36, 136.37 (d, *J*=2.9 Hz), 136.34 (d, *J*=2.9 Hz), 127.6, 127.5, 123.19 (q, *J*=281.0 Hz), 123.17 (q, *J*=281.0 Hz), 120.59 (d, *J*=8.8 Hz), 120.55 (d, *J*=8.1 Hz), 116.14 (d, *J*=22.7 Hz), 116.12 (d, *J*=23.5 Hz), 105.1, 105.0, 72.43 (q, *J*=30.8 Hz), 72.38 (q, *J*=31.5 Hz), 60.1, 49.3, 49.2, 48.7, 48.6, 25.9, 25.14, 25.12, 21.10, 21.05. LCMS *m/z* 400.2 [M + H]+. HRMS (ESI) *m/z* calculated for $C_{18}H_{17}F_4N_3O_3$ [M + H+]: 400.1279. Found 400.1260.

(2R)-1,1,1-Trifluoro-3-methoxypropan-2-yl (*1R,5S,6r*)-6-[1-(4-fluorophenyl)-*1H*-pyrazol-3-yl]-3-azabicyclo[3.1.0]hexane-3-carboxylate (17). (R)-2-(Trifluoromethyl)oxirane (100 mg, 0.892 mmol) was treated with 1 mL of methanol containing 0.75% H_2SO_4 in a sealed vial, and the mixture was heated at 80 °C for 20 h. The solution was carefully concentrated under reduced pressure at ~5 °C to afford 120 mg (93%) of (R)-1,1,1-trifluoro-3-methoxypropan-2-ol as a colorless liquid. The crude product contained residual methanol, but was used without further

purification. ^{1}H NMR (400 MHz, METHANOL-d_4) δ ppm 4.10 (ddq, *J*=7.3, 3.5, 7.3 Hz, 1 H), 3.61 (dd, *J*=10.5, 3.5 Hz, 1 H), 3.50 (dd, *J*=10.5, 7.3 Hz, 1 H), 3.39 (s, 3 H).

Bis(pentafluorophenyl)carbonate (164 mg, 0.42 mmol) and trimethylamine (176 mg, 1.74 mmol) were added to a solution of (R)-1,1,1-trifluoro-3-methoxypropan-2-ol (50 mg, 0.35 mmol) in 2 mL of acetonitrile at room temperature. After stirring for an additional 40 minutes at room temperature, a solution of (*1R,5S,6r*)-6-[1-(4-fluorophenyl)-*1H*-pyrazol-3-yl]-3-azabicyclo[3.1.0]hexane, trifluoroacetate salt (**24**) (140 mg, 0.2 mmol) and triethylamine (102 mg, 1.01 mmol) in 2 mL of acetonitrile was added, and the mixture was stirred at 30 °C for 3 h. The reaction was concentrated at reduced pressure to give a crude residue that was purified by reverse phase preparative HPLC to afford 26 mg (32%) of **17** as a yellow gum. By ^{1}H NMR analysis, the product was judged to be a mixture of rotamers. ^{1}H NMR (400 MHz, $CDCl_3$) δ ppm 7.76-7.72 (m, 1 H), 7.63-7.56 (m, 2 H), 7.17-7.09 (m, 2 H), 6.19 (d, *J*=4.5 Hz, 1 H), 5.49-5.40 (m, 1 H), 3.94-3.80 (m, 2 H), 3.73-3.67 (m, 2 H), 3.65-3.57 (m, 2 H), 3.42 (s, 3H), 2.03 (br s, 2 H), 1.93-1.82 (m, 1 H). ^{13}C NMR (101 MHz, $CDCl_3$) δ 160.9 (d, *J*=245.0 Hz), 153.56, 153.50, 153.19, 153.16, 136.4 (d, *J*=2.9 Hz), 127.6, 127.48, 127.45, 123.3 (q, *J*=281.0 Hz), 120.6 (d, *J*=8.1 Hz), 116.1 (d, *J*=22.7 Hz), 105.2, 105.0, 69.5 (q, *J*=30.8 Hz), 69.4 (q, *J*=31.5 Hz), 69.1 (m, $\underline{C}H_2OMe$), 59.35, 59.30, 49.24, 49.2, 48.58, 48.52, 25.98, 25.21, 21.09, 21.07. LCMS *m/z* 413.9 $[M+H]^+$.

1,1,1-Trifluoro-4-hydroxybutan-2-yl (*1R,5S,6r*)-6-[1-(4-fluorophenyl)-*1H*-pyrazol-3-yl]-3-azabicyclo[3.1.0]hexane-3-carboxylate (18). A solution of tetrabutylammonium fluoride (0.37 mL, 0.37 mmol, 1.0 M in THF) was added dropwise at 0 °C to a solution of 3-(benzyloxy)propanal (191 mg, 1.16 mmol) and trimethyl(trifluoromethyl)silane (281 mg, 1.98 mmol) in 5 mL of THF. The mixture was stirred at 10 °C for 30 min and subsequently treated

with bis(pentafluorophenyl)carbonate (459 mg, 1.16 mmol) and trimethylamine (589 mg, 5.82 mmol). The resulting solution was stirred for an additional 30 min at 10 °C and then treated with a solution of (*1R,5S,6r*)-6-[1-(4-fluorophenyl)-*1H*-pyrazol-3-yl]-3-azabicyclo[3.1.0]hexane, trifluoroacetate salt (**24**) (208 mg, 0.582 mmol) and triethylamine (294 mg, 2.91 mmol) in 2 mL of methylene chloride. The mixture was stirred at 10 °C for 15 h and then concentrated at reduced pressure. The crude residue obtained was purified by flash chromatography on silica (0% to 10% EtOAc in petroleum ether) to afford 157 mg (54%) of

4-(benzyloxy)-1,1,1-trifluorobutan-2-yl (*1R,5S,6r*)-6-[1-(4-fluorophenyl)-*1H*-pyrazol-3-yl]-3-azabicyclo[3.1.0]hexane-3-carboxylate as a yellow gum. By ^{1}H NMR analysis, the product was judged to be a mixture of rotamers. ^{1}H NMR (400 MHz, $CDCl_3$) δ ppm 7.76-7.73 (m, 1 H), 7.62-7.57 (m, 2 H), 7.41-7.25 (m, 5 H), 7.16-7.10 (m, 2 H), 6.19 (d, *J*=2.4 Hz, 0.5 H), 6.15 (d, *J*=2.4 Hz, 0.5 H), 5.50-5.43 (m, 1 H), 4.53 (s, 0.5 x 2 H), 4.51 (s, 0.5 x 2 H), 3.89-3.72 (m, 2 H), 3.66-3.42 (m, 4 H), 2.19-2.07 (m, 1 H), 2.06-1.94 (m, 3 H), 1.83 (t, *J*=3.4 Hz, 0.5 H), 1.75 (t, *J*=3.4 Hz, 0.5 H). LCMS *m/z* 504.2 $[M+H]^+$.

A mixture of 4-(benzyloxy)-1,1,1-trifluorobutan-2-yl (*1R,5S,6r*)-6-[1-(4-fluorophenyl)-*1H*-pyrazol-3-yl]-3-azabicyclo[3.1.0]hexane-3-carboxylate (157 mg, 0.31 mmol) an 10 % Pd/C (40 mg) in 20 mL of methanol was stirred under a hydrogen atmosphere (30 psi) for 30 h. The mixture was filtered, concentrated, and purified by reverse phase preparative HPLC to afford 21 mg (17%) of **18** as a colorless gum. By ^{1}H and ^{13}C NMR analysis, the product was judged to be a mixture of rotamers. ^{1}H NMR (400 MHz, $CDCl_3$) δ ppm 7.76-7.73 (m, 1 H), 7.64-7.55 (m, 2 H), 7.18-7.09 (m, 2 H), 6.20 (d, *J*=2.5 Hz, 0.5 H), 6.18 (d, *J*=2.5 Hz, 0.5 H), 5.39-5.27 (m, 1 H), 3.91-3.80 (m, 2 H), 3.80-3.72 (m, 1 H), 3.67-3.55 (m, 3 H), 2.15-2.00 (m, 3 H), 1.89-1.77 (m, 3 H). ^{13}C NMR (101 MHz, $CDCl_3$) δ 160.93 (d, *J*=245.8 Hz), 160.91 (d, *J*=245.8 Hz), 154.5,

154.4, 153.4, 153.3, 136.43 (d, *J*=2.9 Hz), 136.39 (d, *J*=2.9 Hz), 127.6, 127.5, 124.2 (q, *J*=278.8 Hz), 120.60 (d, *J*=9 Hz), 120.59 (d, *J*=8.1 Hz), 116.18 (d, *J*=23.5 Hz), 116.16 (d, *J*=22.7 Hz), 105.2, 104.9, 68.74 (q, *J*=32.3 Hz), 68.65 (q, *J*=32.3 Hz), 56.8, 49.32, 49.3, 48.8, 48.6, 31.3, 31.2, 25.91, 25.85, 25.2, 21.2, 21.1. LCMS *m/z* 414.2 $[M+H]^+$. HRMS (ESI) *m/z* calculated for $C_{19}H_{19}F_4N_3O_3$ [M + H+]: 414.1435. Found 414.1428.

(2R)-3,3,3-trifluoro-2-hydroxypropyl (*1R,5S,6r*)-6-[1-(4-fluorophenyl)-*1H*-pyrazol-3-yl]-3-azabicyclo[3.1.0]hexane-3-carboxylate (19). A mixture consisting of (2R)-1,1,1-trifluoro-3-hydroxypropan-2-yl (*1R,5S,6r*)-6-[1-(4-fluorophenyl)-*1H*-pyrazol-3-yl]-3-azabicyclo[3.1.0]hexane-3-carboxylate (**15**) (30 mg, 0.075 mmol), saturated $NaHCO_3$ (1 mL), and acetonitrile (2 mL) was stirred at 30 °C for 4 days. The mixture was diluted with methylene chloride, filtered, concentrated, and purified by reverse phase preparative HPLC to afford 20 mg (65%) of **19** as a white solid. By ^1H and ^{13}C NMR analysis, the product was judged to be a mixture of rotamers. ^1H NMR (400 MHz, $CDCl_3$) δ ppm 7.74 (br s, 1 H), 7.62-7.56 (m, 2 H), 7.16-7.10 (m, 2 H), 6.19 (br s, 1 H), 4.50-4.13 (m, 4 H), 3.94-3.74 (m, 2 H), 3.64-3.54 (m, 2 H), 2.04 (br s, 2 H), 1.87-1.81 (m, 1 H). ^{13}C NMR (101 MHz, $CDCl_3$) δ 160.9 (d, *J*=245.0 Hz), 156.13, 156.06, 153.40, 153.39, 136.4 (d, *J*=2.9 Hz), 127.5, 124.0 (q, *J*=283.2 Hz), 120.6 (d, *J*=8.1 Hz), 116.2 (d, *J*=22.7 Hz), 105.18, 105.13, 70.2 (q, *J*=30.8 Hz), 70.1 (q, *J*=31.5 Hz), 64.1 (m, -O<u>C</u>H_2-), 49.22, 49.20, 48.7, 25.98, 25.95, 25.21, 21.15, 21.11. LCMS *m/z* 399.8 $[M+H]^+$.

***tert*-Butyl (*1R,5S,6r*)-6-acetyl-3-azabicyclo[3.1.0]hexane-3-carboxylate (21).** 1-[3-(Dimethylamino)propyl]-3-ethylcarbodiimide hydrochloride (10.1 g, 52.7 mmol) and 1*H*-benzotriazol-1-ol (7.13 g, 52.8 mmol) were added to a 0 °C solution of (*1R,5S,6r*)-3-(*tert*-butoxycarbonyl)-3-azabicyclo[3.1.0]hexane-6-carboxylic acid (**20**) (8.00 g, 35 mmol) in dichloromethane (80 mL), and the reaction mixture was stirred at 0 °C for 30 minutes. A solution

of *N*-methoxymethanamine hydrochloride (6.87 g, 70.4 mmol) and *N,N*-isopropylethylamine (13.6 g, 105 mmol) in dichloromethane (50 mL) was then added drop-wise over a period of 10 minutes, and the reaction mixture was stirred at room temperature (25 °C) for 2 h. After addition of water (100 mL), the mixture was extracted with dichloromethane (3 x 100 mL), and the combined organic layers were washed with water (50 mL) and saturated aqueous sodium chloride solution (50 mL), dried over sodium sulfate, filtered, and concentrated *in vacuo* to provide 9.46 g (100%) of *tert*-butyl (*1R,5S,6r*)-6-[methoxy(methyl)carbamoyl]-3-azabicyclo[3.1.0]hexane-3-carboxylate as a light yellow oil. ^{1}H NMR (400 MHz, $CDCl_3$) δ 3.72 (s, 3H), 3.64 (d, half of AB quartet, *J*=11.2 Hz, 1H), 3.55 (d, half of AB quartet, *J*=11.0 Hz, 1H), 3.49-3.39 (m, 2H), 3.18 (s, 3H), 2.11-1.99 (m, 2H), 1.99-1.91 (br s, 1H), 1.43 (s, 9H).

Methylmagnesium bromide (3.0 M solution in tetrahydrofuran; 23.3 mL, 69.9 mmol) was added in a drop-wise manner to a 0 °C solution of *tert*-butyl (*1R,5S,6r*)-6-[methoxy(methyl)carbamoyl]-3-azabicyclo[3.1.0]hexane-3-carboxylate (9.46 g, 35.0 mmol) in tetrahydrofuran (100 mL). The reaction mixture was stirred at room temperature (25 °C) for 1 h, whereupon it was quenched with saturated aqueous ammonium chloride solution (200 mL) and extracted with ethyl acetate (3 x 100 mL). The combined organic layers were washed sequentially with water (100 mL) and saturated aqueous sodium chloride solution (100 mL), dried over sodium sulfate, filtered, and concentrated *in vacuo* to provide 7.82 g (99%) of **21** as a red solid. ^{1}H NMR (400 MHz, $CDCl_3$) δ 3.62 (d, half of AB quartet, *J*=11.3 Hz, 1H), 3.53 (d, half of AB quartet, *J*=11.3 Hz, 1H), 3.41-3.32 (m, 2H), 2.21 (s, 3H), 2.05-2.01 (m, 2H), 1.77 (dd, *J*=3.0, 2.9 Hz, 1H), 1.39 (s, 9H). ^{13}C NMR (101 MHz, $CDCl_3$) δ 206.2, 154.6, 79.6, 48.0, 47.8, 32.8, 30.9, 28.8, 28.4 (3C), 28.3.

***tert*-Butyl (*1R,5S,6r*)-6-(1H-pyrazol-3-yl)-3-azabicyclo[3.1.0]hexane-3-carboxylate (22).** To a solution of *tert*-butyl (*1R,5S,6r*)-6-acetyl-3-azabicyclo[3.1.0]hexane-3-carboxylate (**21**) (7.82 g, 34.7 mmol) in *N,N*-dimethylformamide (50 mL) was added *N,N*-dimethylformamide dimethyl acetal (12.4 g, 104 mmol), and the reaction mixture was stirred at 110 °C for 16 h. It was then cooled, treated with water (100 mL), and extracted with ethyl acetate (3 x 100 mL). The combined organic layers were washed sequentially with water (3 x 100 mL) and saturated aqueous sodium chloride solution (90 mL), dried over sodium sulfate, filtered, and concentrated under reduced pressure to afford 9.20 g (94%) of *tert*-butyl (*1R,5S,6r*)-6-[(2E)-3-(dimethylamino)prop-2-enoyl]-3-azabicyclo[3.1.0]hexane-3-carboxylate as a red solid. ^{1}H NMR (400 MHz, $CDCl_3$) δ 7.51 (d, *J*=12.7 Hz, 1H), 5.13 (d, *J*=12.7 Hz, 1H), 3.63 (d, half of AB quartet, *J*=11.2 Hz, 1H), 3.54 (d, half of AB quartet, *J*=11.0 Hz, 1H), 3.44-3.36 (m, 2H), 3.15-2.93 (br s, 3H), 2.93-2.70 (br s, 3H), 2.10-1.97 (m, 2H), 1.60 (dd, *J*=2.9, 2.9 Hz, 1H), 1.42 (s, 9H).

Hydrazine hydrate (1.97 g, 39.4 mmol) was added to a solution of *tert*-butyl (*1R,5S,6r*)-6-[(2E)-3-(dimethylamino)prop-2-enoyl]-3-azabicyclo[3.1.0]hexane-3-carboxylate (9.20 g, 32.8 mmol) in ethanol (100 mL), and the reaction mixture was stirred at 80 °C for 16 h. After concentration *in vacuo*, the residue was purified by chromatography on silica gel (Eluents: 9%, then 17%, then 50% ethyl acetate in diethyl ether) to afford 7.00 g (86%) of **22** as a white solid. ^{1}H NMR (400 MHz, $CDCl_3$) δ 7.47 (d, *J*=2.0 Hz, 1H), 6.01 (br d, *J*=1.8 Hz, 1H), 3.78 (d, *J*=10.9 Hz, 1H), 3.69 (d, *J*=11.0 Hz, 1H), 3.51-3.41 (m, 2H), 1.90-1.83 (m, 2H), 1.80 (dd, *J*=3.4, 3.4 Hz, 1H), 1.46 (s, 9H). ^{13}C NMR (101 MHz, $CDCl_3$) δ 155.0, 149.1, 132.6, 101.8, 79.5, 48.4, 48.2, 28.4 (3C), 25.9, 25.1, 19.9. LCMS *m/z* 193.8 $[(M - 2\text{-methylprop-1-ene})+H]^+$.

***tert*-Butyl (*1R,5S,6r*)-6-[1-(4-fluorophenyl)-*1H*-pyrazol-3-yl]-3-azabicyclo[3.1.0]hexane-3-carboxylate (23).** To a 15 °C solution of *tert*-butyl (*1R,5S,6r*)-6-(*1H*-pyrazol-3-yl)-3-azabicyclo[3.1.0]hexane-3-carboxylate (**22**) (4.0 g, 16 mmol) in dichloromethane (300 mL) were added (4-fluorophenyl)boronic acid (2.92 g, 20.9 mmol), copper(II) acetate (4.37 g, 24.1 mmol), pyridine (3.81 g, 48.2 mmol), and 4Å molecular sieves (0.5 g). The reaction mixture was stirred for 18 h at 30 °C, whereupon it was washed with aqueous ammonium hydroxide solution (100 mL). This aqueous layer was extracted with dichloromethane (2 x 100 mL), and the combined organic layers were washed with saturated aqueous sodium chloride solution (150 mL), dried over sodium sulfate, filtered, and concentrated *in vacuo*. Silica gel chromatography (Gradient: 0% to 25% ethyl acetate in petroleum ether) provided 3.3 g (60%) of **23** as a white solid. ^{1}H NMR (400 MHz, $CDCl_3$) δ 7.73 (d, *J*=2.5 Hz, 1H), 7.62-7.56 (m, 2H), 7.12 (br dd, *J*=8.9, 8.4 Hz, 2H), 6.16 (d, *J*=2.4 Hz, 1H), 3.80 (d, half of AB quartet, *J*=11.0 Hz, 1H), 3.71 (d, half of AB quartet, *J*=10.9 Hz, 1H), 3.52-3.42 (m, 2H), 1.99-1.90 (m, 2H), 1.85 (dd, *J*=3.4, 3.4 Hz, 1H), 1.47 (s, 9H). ^{13}C NMR (101 MHz, $CDCl_3$) δ 160.8 (d, *J*=245.8 Hz), 155.0, 154.1, 136.5 (d, *J*=2.9 Hz), 127.4, 120.5 (d, *J*=8.1 Hz), 116.1 (d, *J*=22.7 Hz), 105.0, 79.4, 48.5, 48.2, 28.5 (3C), 26.2, 25.4, 20.9. LCMS *m/z* 287.8 $[(M - 2\text{-methylprop-1-ene})+H]^+$.

(*1R,5S,6r*)-6-[1-(4-Fluorophenyl)-*1H*-pyrazol-3-yl]-3-azabicyclo[3.1.0]hexane, trifluoroacetate salt (24). A mixture of *tert*-butyl (*1R,5S,6r*)-6-[1-(4-fluorophenyl)-*1H*-pyrazol-3-yl]-3-azabicyclo[3.1.0]hexane-3-carboxylate (**23**) (1.0 g, 2.9 mmol) in trifluoroacetic acid (10 mL) was stirred for 30 minutes at 15 °C, whereupon it was concentrated *in vacuo*. The residue was triturated with *tert*-butyl methyl ether (10 mL) to provide crude **24** as a white solid in quantitative yield. The crude product was used without additional purification. ^{1}H NMR (400 MHz, DMSO-d_6) δ 9.23 (br. s., 1 H), 8.65 (br. s., 1 H), 8.38 (d, *J*=2.7 Hz, 1 H), 7.77 - 7.84 (m, 2

H), 7.69 - 7.88 (m, 2 H), 7.29 - 7.37 (m, 2 H), 6.33 (d, *J*=2.7 Hz, 1 H), 3.49 (dd, *J*=11.7, 6.2 Hz, 2 H), 3.35 - 3.46 (m, 2 H), 2.09 - 2.18 (m, 3 H). LCMS *m/z* 243.9 $[M+H]^+$.

Synthesis of (2R)-1,1,1-Trifluoro-3-(4-methoxybenzyloxy)propan-2-ol (27). To a solution of 4-methoxybenzyl alcohol (37.0 g, 268 mmol) in THF (500 mL) at 0 °C was added NaH (21.4 g, 535 mmol, 60%) portionwise. The solution was stirred at 0 °C for 1 h and treated with 2-(trifluoromethyl)oxirane (20.0 g, 178.5 mmol). The resulting mixture was stirred at rt overnight. This reaction was run three times on identical scale. The three reactions were combined, cooled to 0 °C, quenched with water, and extracted with EtOAc (3 x 1000 mL). The combined organic extracts were dried (Na_2SO_4), filtered, and concentrated. The crude residue obtained was purified by silica gel chromatography (Gradient: 5% to 25% EtOAc in petroleum ether) to afford 114.4 g of racemic 1,1,1-trifluoro-3-(4-methoxybenzyloxy)propan-2-ol as a yellow oil. Further purification by chiral supercritical fluid chromatography (Isocratic: 92.5% CO_2/7.5 % MeOH; Chiral Tech AS-H 250mm x 4.6 mm) gave 31.6 g (41%) of (R)- 1,1,1-trifluoro-3-(4-methoxybenzyloxy)propan-2-ol as the first eluting isomer and 32.7 g (43%) of (S)- 1,1,1-trifluoro-3-(4-methoxybenzyloxy)propan-2-ol as the second eluting isomer.

Spectral data for (2R)- 1,1,1-trifluoro-3-(4-methoxybenzyloxy)propan-2-ol (**27**):

^{1}H NMR (400 MHz, $CDCl_3$) δ ppm 7.27 (d, *J*=8.6 Hz, 2 H), 6.91 (d, *J*=8.6 Hz, 2 H), 4.53 (s, 2 H), 4.18 - 4.07 (m, 1 H), 3.82 (s, 3 H), 3.71 (dd, *J*=10.1, 3.7, 1 H), 3.63 (dd, *J*=10.1, 6.2 Hz, 1 H). ^{13}C NMR (101 MHz, $CDCl_3$) δ 159.5, 129.5, 129.0, 124.2 (q, *J*=281.7 Hz), 114.0, 73.4, 69.4 (q, *J*=31.5 Hz), 67.1 (q, *J*=2.2 Hz), 55.2. $[\alpha]_D^{20}$ +6.2° (*c* 1.58, MeOH).

Spectral data for (2S)- 1,1,1-trifluoro-3-(4-methoxybenzyloxy)propan-2-ol:

^{1}H NMR (400 MHz, $CDCl_3$) δ ppm 7.27 (d, *J*=8.6 Hz, 2 H), 6.91 (d, *J*=8.6 Hz, 2 H), 4.55 (d, *J*=11.4 Hz, 1 H), 4.52 (d, *J*=11.4 Hz, 1 H), 4.18 - 4.07 (m, 1 H), 3.82 (s, 3 H), 3.71 (dd, *J*=10.1, 3.7, 1 H), 3.63 (dd, *J*=10.1, 6.2 Hz, 1 H). $[\alpha]_D^{20}$ -5.8° (*c* 1.55, MeOH).

Modeling Studies

The binding site model used for MAGL docking was based on the published X-ray coordinates of MAGL (PDB: 3PE6). Protein side chains within a 5 Å radius of the bound ligand were allowed to relax to reorient in order to optimize binding interactions using the Induced Fit protocol in the Schrodinger package.[52] The solution with the best docking score was chosen and used for analysis.

X-ray structure of MAGL Bound to compound 10

Crystals of the complex of Compound **10** and human MAGL were obtained by soaking apo crystals into a 1mM solution of the compound following protocols described earlier.[45]

X-ray diffraction data to 2.0 Å resolution were collected at 100K with radiation of wavelength 1 Å at beamline 08-ID of the Canadian Light Source in Saskatchewan, Canada, on Mar300 CCD detector. Data processing, merging and scaling were done with the program HKL2000.[56] The structure was solved by molecular replacement using PDB entry 3HJU[57] as the search model, and refined with autoBUSTER[58]. Model building and fitting was done using Coot[59]. Data collection and refinement statistics are given in Table S1.

Atomic coordinates and structure factors have been deposited in the Protein Data Bank with the accession code 6BQ0.

In Vitro Pharmacology

Assessment of MAGL inhibition (MAGL IC_{50}): Assessment of MAGL inhibition utilizes human recombinant Monoacylglycerol Lipase and the fluorogenic substrate 7-hydroxycoumarinyl arachidonate (7-HCA, Biomol ST-502). 400 nL of a test compound at decreasing concentration (ranging from 150 μM down to 1.5 nM) was spotted into a 384-well back plate (PerkinElmer, 6007279) using a Labcyte Echo, followed by addition of 10 μL of MAGL enzyme in assay buffer (50mM HEPES, pH 7.4, 100 mM NaCl, 5 mM $MgCl_2$, 0.1% Triton X-100 and 25% glycerin). An equal volume of 7-HCA in assay buffer with 10% DMSO was added either immediately (T = 0 min) or after a 30 min incubation (T = 30 min) to initiate the reaction. The final concentration of MAGL enzyme was 88 pM and 7-HCA substrate was 5 μM. After these dilutions, the final concentration of the test compound ranged from 3 μM to 0.03 nM. The reaction was allowed to progress for 60 minutes, after which the plate was read at an Ex/Em of 340/465. Percent inhibitions were calculated based on control wells containing no compound (0% inhibition) and a control compound (e.g., a MAGL inhibitor whose activity is known or was previously reported in the literature, such as one with about 100% inhibition). IC_{50} values were generated based on a four parameter fit model using ABASE software from IDBS. See e.g., Wang, Y. et al., "A Fluorescence-Based Assay for Monoacylglycerol Lipase Compatible with Inhibitor Screening," Assay and Drug Development Technologies, 2008, Vol. 6 (3) pp 387-393 (reporting an assay for measuring MAGL activity).[46]

Assessment of rate of MAGL inactivation (MAGL k_{inact}/K_I): To measure MAGL inactivation, the same protocol for the (T = 0 min) MAGL inhibition IC_{50} assay was performed with data collected every minute to acquire enzyme progress curves at decreasing concentrations of

compound. K_{obs} values were calculated from this data and k_{inact}/K_i ratios were determined from a plot of K_{obs} values vs. compound concentrations.

Assessment of FAAH inhibition: Assessment of FAAH inhibition utilizes human recombinant Fatty Acid Amide Hydrolase Lipase and the fluorogenic substrate, Arachidonoyl-AMC (Sigma A6855). 400 nL of a test compound at decreasing concentration was spotted into a 384-well back plate (PerkinElmer, 6007279) using a Labcyte Echo, followed by addition of 10µl of FAAH enzyme(Cayman 10010183) in assay buffer (50mM Tris, pH 9.0, 1mM EDTA). After a 30 minute incubation at room temperature, 10µL of Arachidonyl-AMC was added in assay buffer with 16% DMSO. Final concentration of FAAH enzyme was 0.0125 Units and the AAMC substrate was used at a concentration of 5µM. The final concentration of the test compound ranged from 30 µM to 0.3 nM. The reaction was allowed to progress for 60 minutes, after which the plate was read at an Ex/Em of 355/460. Percent inhibitions were calculated based on control wells containing no compound (0% inhibition) and a control compound at a concentration known to inhibit FAAH to 100%. IC50 values were generated based on a four parameter fit model using ABASE software from IDBS.

In Vivo Pharmacokinetic studies

The pharmacokinetic studies in rat, dog, and non-human primate (nhp) were conducted at Pfizer Global Research and Development (Groton, CT). All in vivo studies were conducted in accordance with regulations and established guidelines using protocols reviewed and approved by the Pfizer Worldwide Research and Development (WRD) Institutional Animal Care and Use Committee. For all species, blood samples were collected into tubes containing EDTA fortified with PMSF at a final concentration of 10 mM and placed on wet ice (phenylmethylsulfonyl

fluoride; stock solution prepared in DMSO at 1 M and aliquoted into blood collection tubes prior to blood collection a ratio of 1:100). Following centrifugation to afford plasma, the samples were transferred to polypropylene tubes and stored frozen at –20°C to –80°C until analysis.

Rat intravenous pharmacokinetic study: Dual cannulated (jugular vein and carotid artery) male Wistar Hannover rats (250-300 g; Charles River Laboratories, Wilmington, MA) were maintained on a 12-h light/dark cycle for a minimum of three days in a temperature- and humidity-controlled environment with food and water provided ad libitium. The rats (n = 2) were administered an intravenous (IV) bolus of Compound **15** at 1 mg/kg via a jugular vein cannula. The IV dose was a solution formulated in 3% DMA/10% Solutol HS15/10% Miglyol/77% 20% SBECD in water and delivered at a 1 mL/kg dose volume. Serial blood samples were collected from each rat via a carotid artery cannula prior to dose administration and at the following time points post-dose: 0.083, 0.25, 0.5, 1, 2, 4, 7, and 24 h.

Dog intravenous pharmacokinetic study: Male beagle dogs were fasted overnight with water provided ad libitium. The dogs were fed at approximately 4 h post-dose. The dogs (n = 2) were administered an IV bolus of Compound **15** at 1 mg/kg via the cephalic vein. The IV dose was a solution formulated in 3% DMA/10% Solutol HS15/10% Miglyol/77% 20% SBECD in water and delivered at a 0.5 mL/kg dose volume. Serial blood samples were collected from each dog via the jugular vein prior to dose administration and at the following time points post-dose: 0.083, 0.25, 0.5, 1, 2, 4, 7, and 24 h.

Nhp intravenous pharmacokinetic study: Male nhps were fasted overnight with water provided ad libitium. The nhps were fed at approximately 1 h post-dose. The nhps (n = 2) were administered an IV bolus of Compound **15** at 1 mg/kg via either the saphenous vein or the

cephalic vein. The IV dose was a solution formulated in 3% DMA/10% Solutol HS15/10% Miglyol/77% 20% SBECD in water and delivered at a 0.5 mL/kg dose volume. Serial blood samples were collected from each nhp via the femoral vein prior to dose administration and at the following time points post-dose: 0.083, 0.25, 0.5, 1, 2, 4, 7, and 24 h.

Analysis of compound in plasma and pharmacokinetic parameters: All plasma samples were quantified via HPLC-MS/MS using non-validated methods. The plasma standard curves were prepared separately for each species and were generated with species specific plasma that was prepared in the same manner as the samples to obtain control plasma fortified with PMSF from whole blood. Pharmacokinetic parameters were determined by non-compartmental analysis using Watson LIMS software version 7.4 (Thermo Fisher Scientific, Waltham, MA).

In Vivo Pharmacokinetic and Pharmacodynamics Studies

All procedures performed on animals in this study were in accordance with established guidelines and regulations, and were reviewed and approved by the Pfizer (or other) Institutional Animal Care and Use Committee or through an ethical review process.

Pharmacokinetic and Pharmacodynamic Assessment: Compound **15** was dissolved in vehicle (5:5:90 DMSO:Cremophor:Saline) and a 1 mg/kg dose was administered subcutaneously at a dose volume of 10 mL/kg to male C57BL6J mice. Plasma and brain samples were collected at given time points (0.5, 1, 2, 4, 8, 12 and 24 h). Drug concentrations were measured in plasma and cerebellum while 2-AG and AA was assessed in brain hemisphere as previously described.[45]

LPS Induced Inflammation: A 4 mg/mL solution of LPS (0127:B8 from Escherichia coli; Sigma Aldrich Cat. No. L3129 St. Louis, MO) was made by dissolving into sterile saline. Solution was vortexed and gently heated until LPS was fully dissolved. Mice were intraperitoneally

administered 5 mL/kg of LPS (20 mg/kg final) or saline. At 30 min post LPS injection mice were subcutaneously administered vehicle (5:5:90 DMSO:Cremophor:Saline) or 1 mg/kg compound 9. Brain samples were collected at 4 hours post LPS dosing. Mice were anesthetized with isoflurane followed by euthanasia via cervical dislocation. Brains were rapidly removed (less than 30 seconds) and dissected into two hemi-brains (1 used for pharmacodynamic measurement and 1 used for cytokine measurement). Brains were immediately frozen in liquid nitrogen and stored at -80°C until analysis.

PGE2 Measurement: Brain samples were prepared on wet ice. Briefly, brain homogenates were prepared by homogenizing brain with 3 volumes (w:v) of homogenization buffer (1% 100 mM PMSF and 5% 100 mM NH_4OAc in water pH 2.0, adjusted with formic acid). The brain homogenates were then further diluted 3:1 (v:v) in homogenizing buffer. Samples were then spiked with IS solution [300 pg/mL d_4-PGE2 (Cayman Chemical, Ann Arbor, Michigan) in acetonitrile (ACN)] followed by precipitation and organic extraction in ACN. Samples were then centrifuged at 15,700 rcf for 15 min at 4°C. Supernatant was removed from each sample and directly injected for LC-MS/MS analysis. The PGE2 calibration curve consisted of 0.391-200 ng/mL. Samples were directly injected onto a Waters BEH300 C-18 HPLC column. Mass spectrometry was run in negative ESI mode with SRM detection. The PGE2 *m/z* was 351.2/271.3. The d_4-PGE2 *m/z* was 355.2/275.2.

Brain Cytokine Measurement: Brain samples were prepared on wet ice. Hemi-brains were homogenized in phosphate buffered saline (PBS) with protease inhibitors (cOmplete EDTA-free, Roche, Indianapolis, IN) using a TissueLyser II (Qiagen, Germantown, MD) and 5 mm stainless steel beads. Brain tissue was homogenized at 25 hertz for 4 min at 4°C followed by incubation on ice for 15 min. Samples were then centrifuged at 100,000 rcf for 45 min at 4°C. Supernatant

was then removed and split into two aliquots. One aliquot was frozen at -80°C for cytokine measurement and the other was used to determine the total protein concentration of the sample. Protein concentration was determined using the BCA protein assay kit (Thermo Fisher, Waltham, MA) according to the manufacturer's directions.

Brain cytokines were measured using the mouse Proinflammatory Panel 1 custom analysis for IL1β, IL6 and TNFα (Meso Scale Discovery No K152AOH-2, Rockville, MD). The frozen aliquot of brain supernatant was thawed on ice prior to being diluted into Diluent 41. Saline treated samples were diluted 1:2 and LPS treated samples were diluted 1:4. Cytokines were then measured according to the manufacturer's directions.

ASSOCIATED CONTENT

SUPPORTING INFORMATION

The Supporting Information is available free of charge on the
ACS Publications website at DOI:

Data Processing & Model Refinement Statistics for MAGL complex with **10**, Experimental protocol for serine hydrolase selectivity profiling by competitive activity based protein profiling (ABPP), Full serine hydrolase panel activity for MAGL Inhibitors **8**, **10** and **15** at 10μM, MAGL and FAAH IC_{50} data with confidence intervals (PDF), Molecular formula strings (CSV).

PDB ID Codes: The coordinate data for the co-crystal structure of compound **10** with MAGL have been deposited in the Protein Data Bank with accession number 6BQ0. Authors will release the atomic coordinates and experimental data upon article publication.

AUTHOR INFORMATION

Corresponding Author

*To whom correspondence should be addressed. Email: laura.mcallister@pfizer.com. Phone: +1 617-395-0862

Note: The authors declare the following competing financial interest(s): All authors were employed by Pfizer, Inc. at the time this work was done.

ABBREVIATIONS

AA, arachidonic acid; ABPP, activity based protein profiling; ACB, acyl chain binding, 2-AG, 2-arachidonoylglycerol; BCRP, breast cancer resistance protein; CA, cytoplasmic access; CNS, central nervous system; COX, cyclooxygenase; FAAH, fatty acid amide hydrolase; HFIP, hexafluoroisopropanol; IADR, idiosyncratic adverse drug reaction; IL1b, Interleukin 1 beta; LipE, lipophilic efficiency; LPS, lipopolysaccharide; MAGL, monoacylglycerol lipase; PGE2, Prostaglandin E_2; PGP, P-glycoprotein; cPLA2, cytosolic phospholipase A2; TNFa, tumor necrosis factor alpha.

REFERENCES

1. Dinh, T. P.; Freund, T. F.; Piomelli, D. A role for monoglyceride lipase in 2-arachidonoylglycerol inactivation. *Chem. Phys. Lipids* **2002,** *121,* 149-158.

2. Marnett, L. J. Decoding endocannabinoid signaling. *Nat. Chem. Biol.* **2009,** *5,* 8-9.

3. Savinainen, J. R.; Saario, S. M.; Laitinen, J. T. The serine hydrolases MAGL, ABHD6 and ABHD12 as guardians of 2-arachidonoylglycerol signalling through cannabinoid receptors. *Acta Physiol. (Oxf)* **2012,** *204,* 267-276.

4. Fowler, C. J. Monoacylglycerol lipase - a target for drug development? *Br. J. Pharmacol.* **2012,** *166,* 1568-1585.

5. Long, J. Z.; Cravatt, B. F. The metabolic serine hydrolases and their functions in mammalian physiology and disease. *Chem. Rev.* **2011,** *111,* 6022-6063.

6. Chanda, P. K.; Gao, Y.; Mark, L.; Btesh, J.; Strassle, B. W.; Lu, P.; Piesla, M. J.; Zhang, M. Y.; Bingham, B.; Uveges, A.; Kowal, D.; Garbe, D.; Kouranova, E. V.; Ring, R. H.; Bates, B.; Pangalos, M. N.; Kennedy, J. D.; Whiteside, G. T.; Samad, T. A. Monoacylglycerol lipase activity is a critical modulator of the tone and integrity of the endocannabinoid system. *Mol. Pharmacol.* **2010,** *78,* 996-1003.

7. Nomura, D. K.; Morrison, B. E.; Blankman, J. L.; Long, J. Z.; Kinsey, S. G.; Marcondes, M. C.; Ward, A. M.; Hahn, Y. K.; Lichtman, A. H.; Conti, B.; Cravatt, B. F. Endocannabinoid hydrolysis generates brain prostaglandins that promote neuroinflammation. *Science* **2011,** *334,* 809-813.

8. Mulvihill, M. M.; Nomura, D. K. Therapeutic potential of monoacylglycerol lipase inhibitors. *Life Sci.* **2013,** *92,* 492-497.

9. Bachovchin, D. A.; Cravatt, B. F. The pharmacological landscape and therapeutic potential of serine hydrolases. *Nat. Rev. Drug Discov.* **2012,** *11,* 52-68.

10. Grabner, G. F.; Zimmermann, R.; Schicho, R.; Taschler, U. Monoglyceride lipase as a drug target: At the crossroads of arachidonic acid metabolism and endocannabinoid signaling. *Pharmacol. Ther.* **2017,** *175,* 35-46.

11. da Fonseca, A. C. C.; Matias, D.; Garcia, C.; Amaral, R.; Geraldo, L. H.; Freitas, C.; Lima, F. R. S. The impact of microglial activation on blood-brain barrier in brain diseases. *Front. Cell. Neurosci.* **2014,** *8,* 362.

12. Ransohoff, R. M. How neuroinflammation contributes to neurodegeneration. *Science* **2016,** *353,* 777-783.

13. Piro, J. R.; Benjamin, D. I.; Duerr, J. M.; Pi, Y.; Gonzales, C.; Wood, K. M.; Schwartz, J. W.; Nomura, D. K.; Samad, T. A. A dysregulated endocannabinoid-eicosanoid network supports pathogenesis in a mouse model of Alzheimer's disease. *Cell Rep.* **2012,** *1,* 617-623.

14. Pasquarelli, N.; Porazik, C.; Bayer, H.; Buck, E.; Schildknecht, S.; Weydt, P.; Witting, A.; Ferger, B. Contrasting effects of selective MAGL and FAAH inhibition on dopamine depletion and GDNF expression in a chronic MPTP mouse model of Parkinson's disease. *Neurochem. Int.* **2017,** *110,* 14-24.

15. Hernandez-Torres, G.; Cipriano, M.; Heden, E.; Bjorklund, E.; Canales, A.; Zian, D.; Feliu, A.; Mecha, M.; Guaza, C.; Fowler, C. J.; Ortega-Gutierrez, S.; Lopez-Rodriguez, M. L. A reversible and selective inhibitor of monoacylglycerol lipase ameliorates multiple sclerosis. *Angew. Chem. Int. Ed. Engl.* **2014,** *53,* 13765-13770.

16. Kinsey, S. G.; Wise, L. E.; Ramesh, D.; Abdullah, R.; Selley, D. E.; Cravatt, B. F.; Lichtman, A. H. Repeated low-dose administration of the monoacylglycerol lipase inhibitor JZL184 retains cannabinoid receptor type 1-mediated antinociceptive and gastroprotective effects. *J. Pharmacol. Exp. Ther.* **2013,** *345,* 492-501.

17. Ignatowska-Jankowska, B.; Wilkerson, J. L.; Mustafa, M.; Abdullah, R.; Niphakis, M.; Wiley, J. L.; Cravatt, B. F.; Lichtman, A. H. Selective monoacylglycerol lipase inhibitors: antinociceptive versus cannabimimetic effects in mice. *J. Pharmacol. Exp. Ther.* **2015,** *353,* 424-432.

18. Brindisi, M.; Maramai, S.; Gemma, S.; Brogi, S.; Grillo, A.; Di Cesare Mannelli, L.; Gabellieri, E.; Lamponi, S.; Saponara, S.; Gorelli, B.; Tedesco, D.; Bonfiglio, T.; Landry, C.; Jung, K. M.; Armirotti, A.; Luongo, L.; Ligresti, A.; Piscitelli, F.; Bertucci, C.; Dehouck, M. P.; Campiani, G.; Maione, S.; Ghelardini, C.; Pittaluga, A.; Piomelli, D.; Di Marzo, V.; Butini, S. Development and pharmacological characterization of selective blockers of 2-arachidonoyl glycerol degradation with efficacy in rodent models of multiple sclerosis and pain. *J. Med. Chem.* **2016,** *59,* 2612-2632.

19. Schurman, L. D.; Lichtman, A. H. Endocannabinoids: A promising impact for traumatic brain injury. *Front. Pharmacol.* **2017,** *8,* 69.

20. Long, J. Z.; Nomura, D. K.; Cravatt, B. F. Characterization of monoacylglycerol lipase inhibition reveals differences in central and peripheral endocannabinoid metabolism. *Chem. Biol.* **2009,** *16,* 744-753.

21. Chiurchiù, V.; Battistini, L.; Maccarrone, M. Endocannabinoid signalling in innate and adaptive immunity. *Immunology* **2015,** *144,* 352-364.

22. Bertrand, T.; Auge, F.; Houtmann, J.; Rak, A.; Vallee, F.; Mikol, V.; Berne, P. F.; Michot, N.; Cheuret, D.; Hoornaert, C.; Mathieu, M. Structural basis for human monoglyceride lipase inhibition. *J. Mol. Biol.* **2010,** *396,* 663-673.

23. Singh, J.; Petter, R. C.; Baillie, T. A.; Whitty, A. The resurgence of covalent drugs. *Nat. Rev. Drug Discov.* **2011,** *10,* 307-317.

24. Granchi, C.; Rizzolio, F.; Palazzolo, S.; Carmignani, S.; Macchia, M.; Saccomanni, G.; Manera, C.; Martinelli, A.; Minutolo, F.; Tuccinardi, T. Structural optimization of 4-chlorobenzoylpiperidine derivatives for the development of potent, reversible, and selective monoacylglycerol lipase (magl) inhibitors. *J. Med. Chem.* **2016,** *59,* 10299-10314.

25. Aghazadeh Tabrizi, M.; Baraldi, P. G.; Baraldi, S.; Ruggiero, E.; De Stefano, L.; Rizzolio, F.; Di Cesare Mannelli, L.; Ghelardini, C.; Chicca, A.; Lapillo, M.; Gertsch, J.; Manera, C.; Macchia, M.; Martinelli, A.; Granchi, C.; Minutolo, F.; Tuccinardi, T. Discovery of 1,5-diphenylpyrazole-3-carboxamide derivatives as potent, reversible, and selective monoacylglycerol lipase (magl) inhibitors. *J. Med. Chem.* **2018,** *61,* 1340-1354.

26. Long, J. Z.; Li, W.; Booker, L.; Burston, J. J.; Kinsey, S. G.; Schlosburg, J. E.; Pavon, F. J.; Serrano, A. M.; Selley, D. E.; Parsons, L. H.; Lichtman, A. H.; Cravatt, B. F. Selective blockade of 2-arachidonoylglycerol hydrolysis produces cannabinoid behavioral effects. *Nat. Chem. Biol.* **2009,** *5,* 37-44.

27. Chang, J. W.; Niphakis, M. J.; Lum, K. M.; Cognetta, A. B., 3rd; Wang, C.; Matthews, M. L.; Niessen, S.; Buczynski, M. W.; Parsons, L. H.; Cravatt, B. F. Highly selective inhibitors of monoacylglycerol lipase bearing a reactive group that is bioisosteric with endocannabinoid substrates. *Chem. Biol.* **2012,** *19,* 579-588.

28. Griebel, G.; Pichat, P.; Beeske, S.; Leroy, T.; Redon, N.; Jacquet, A.; Francon, D.; Bert, L.; Even, L.; Lopez-Grancha, M.; Tolstykh, T.; Sun, F.; Yu, Q.; Brittain, S.; Arlt, H.; He, T.; Zhang, B.; Wiederschain, D.; Bertrand, T.; Houtmann, J.; Rak, A.; Vallee, F.; Michot, N.; Auge, F.; Menet, V.; Bergis, O. E.; George, P.; Avenet, P.; Mikol, V.; Didier, M.; Escoubet, J. Selective blockade of the hydrolysis of the endocannabinoid 2-arachidonoylglycerol impairs learning and memory performance while producing antinociceptive activity in rodents. *Sci. Rep.* **2015,** *5,* 7642.

29. Niphakis, M. J.; Cognetta, A. B., 3rd; Chang, J. W.; Buczynski, M. W.; Parsons, L. H.; Byrne, F.; Burston, J. J.; Chapman, V.; Cravatt, B. F. Evaluation of NHS carbamates as a potent and selective class of endocannabinoid hydrolase inhibitors. *ACS Chem. Neurosci.* **2013,** *4,* 1322-1332.

30. Cisar, J. S.; Grice, C. A.; Jones, T. K.; Weber, O. D.; Wang, D.-H. Preparation of Piperazine Carbamates as Modulators of MAGL and/or ABHD6. WO2016149401, 2016.

31. Cisar, J. S.; Grice, C. A.; Jones, T. K.; Wang, D.-H.; Weber, O.; Cravatt, B. F.; Niphakis, M. J.; Cognetta, A.; Chang, J. W. Preparation of Carbamate Compounds as Modulators of MAGL and/or ABHD6. WO2013142307, 2013.

32. Bartsch, R.; Cheuret, D.; Even, L.; Hoornaert, C.; Jeunesse, J.; Marguet, F. Hexafluoroisopropyl Carbamate Derivatives, Especially Aryl- and Heteroaryl-Piperidinecarboxylates and Analogs, their Preparation and Use as Selective Monoacyl Glycerol Lipase (MGL) Inhibitors or Mixed MGL and Fatty Acid Amide Hydrolase Inhibitors. WO2011151808, 2011.

33. Aaltonen, N.; Savinainen, J. R.; Ribas, C. R.; Ronkko, J.; Kuusisto, A.; Korhonen, J.; Navia-Paldanius, D.; Hayrinen, J.; Takabe, P.; Kasnanen, H.; Pantsar, T.; Laitinen, T.; Lehtonen, M.; Pasonen-Seppanen, S.; Poso, A.; Nevalainen, T.; Laitinen, J. T. Piperazine and piperidine triazole ureas as ultrapotent and highly selective inhibitors of monoacylglycerol lipase. *Chem. Biol.* **2013,** *20,* 379-390.

34. Patel, J. Z.; Ahenkorah, S.; Vaara, M.; Staszewski, M.; Adams, Y.; Laitinen, T.; Navia-Paldanius, D.; Parkkari, T.; Savinainen, J. R.; Walczynski, K.; Laitinen, J. T.; Nevalainen, T. J. Loratadine analogues as MAGL inhibitors. *Bioorg. Med. Chem. Lett.* **2015,** *25,* 1436-1442.

35. Blankman, J. L.; Clapper, J. R.; Ezekowitz, R. A. B.; Fraser, I. P.; Grice, C. A.; Jones, T. K.; O'Neill, G. P.; Thurston, A. W., Jr.; Beals, C. R. Methods of Treating Inflammation or Neuropathic Pain Using the Monoacylglycerol Lipase Inhibitor 1,1,1,3,3,3-Hexafluoropropan-2-yl-4-(2-(pyrrolidin-1-yl)-4-(trifluoromethyl)benzyl)piperazine-1-carboxylate. WO2016183097, 2016.

36. Granchi, C.; Caligiuri, I.; Minutolo, F.; Rizzolio, F.; Tuccinardi, T. A patent review of Monoacylglycerol Lipase (MAGL) inhibitors (2013-2017). *Expert Opin. Ther. Pat.* **2017,** 1-11.

37. Wager, T. T.; Chandrasekaran, R. Y.; Hou, X.; Troutman, M. D.; Verhoest, P. R.; Villalobos, A.; Will, Y. Defining desirable central nervous system drug space through the alignment of molecular properties, in vitro ADME, and safety attributes. *ACS Chem. Neurosci.* **2010,** *1,* 420-434.

38. Ryckmans, T.; Edwards, M. P.; Horne, V. A.; Correia, A. M.; Owen, D. R.; Thompson, L. R.; Tran, I.; Tutt, M. F.; Young, T. Rapid assessment of a novel series of selective CB(2) agonists using parallel synthesis protocols: A Lipophilic Efficiency (LipE) analysis. *Bioorg. Med. Chem. Lett.* **2009,** *19,* 4406-4409.

39. Wager, T. T.; Hou, X.; Verhoest, P. R.; Villalobos, A. Moving beyond rules: the development of a central nervous system multiparameter optimization (CNS MPO) approach to enable alignment of druglike properties. *ACS Chem. Neurosci.* **2010,** *1,* 435-449.

40. Chang, J. W.; Cognetta, A. B., 3rd; Niphakis, M. J.; Cravatt, B. F. Proteome-wide reactivity profiling identifies diverse carbamate chemotypes tuned for serine hydrolase inhibition. *ACS. Chem. Biol.* **2013,** *8,* 1590-1599.

41. Johnson, D. S.; Weerapana, E.; Cravatt, B. F. Strategies for discovering and derisking covalent, irreversible enzyme inhibitors. *Future Med. Chem.* **2010,** *2,* 949-964.

42. Stepan, A. F.; Walker, D. P.; Bauman, J.; Price, D. A.; Baillie, T. A.; Kalgutkar, A. S.; Aleo, M. D. Structural alert/reactive metabolite concept as applied in medicinal chemistry to mitigate the risk of idiosyncratic drug toxicity: a perspective based on the critical examination of trends in the top 200 drugs marketed in the United States. *Chem. Res. Toxicol.* **2011,** *24,* 1345-1410.

43. Kalgutkar, A. S.; Dalvie, D. Predicting toxicities of reactive metabolite-positive drug candidates. *Annu. Rev. Pharmacol. Toxicol.* **2015,** *55,* 35-54.

44. Dahal, U. P.; Obach, R. S.; Gilbert, A. M. Benchmarking in vitro covalent binding burden as a tool to assess potential toxicity caused by nonspecific covalent binding of covalent drugs. *Chem. Res. Toxicol.* **2013,** *26,* 1739-1745.

45. Butler, C. R.; Beck, E. M.; Harris, A.; Huang, Z.; McAllister, L. A.; Am Ende, C. W.; Fennell, K.; Foley, T. L.; Fonseca, K.; Hawrylik, S. J.; Johnson, D. S.; Knafels, J. D.; Mente, S.; Noell, G. S.; Pandit, J.; Phillips, T. B.; Piro, J. R.; Rogers, B. N.; Samad, T. A.; Wang, J.; Wan, S.; Brodney, M. A. Azetidine and piperidine carbamates as efficient, covalent inhibitors of monoacylglycerol lipase. *J. Med. Chem.* **2017,** *60,* 9860-9873.

46. Wang, Y.; Chanda, P.; Jones, P. G.; Kennedy, J. D. A fluorescence-based assay for monoacylglycerol lipase compatible with inhibitor screening. *Assay Drug Dev. Technol.* **2008,** *6,* 387-393.

47. Mileni, M.; Johnson, D. S.; Wang, Z.; Everdeen, D. S.; Liimatta, M.; Pabst, B.; Bhattacharya, K.; Nugent, R. A.; Kamtekar, S.; Cravatt, B. F.; Ahn, K.; Stevens, R. C. Structure-guided inhibitor design for human FAAH by interspecies active site conversion. *Proc. Nat.l Acad. Sci. U. S. A.* **2008,** *105,* 12820-12824.

48. Lang, W.; Qin, C.; Lin, S.; Khanolkar, A. D.; Goutopoulos, A.; Fan, P.; Abouzid, K.; Meng, Z.; Biegel, D.; Makriyannis, A. Substrate specificity and stereoselectivity of rat brain microsomal anandamide amidohydrolase. *J. Med. Chem.* **1999,** *42,* 896-902.

49. Lombardo, F.; Shalaeva, M. Y.; Tupper, K. A.; Gao, F. ElogD(oct): a tool for lipophilicity determination in drug discovery. 2. Basic and neutral compounds. *J. Med. Chem.* **2001,** *44,* 2490-2497.

50. Stopher, D.; McClean, S. An improved method for the determination of distribution coefficients. *J. Pharm. Pharmacol.* **1990,** *42,* 144.

51. Chung, J. Y. L. Trifluoromethyloxirane. e-EROS Encyclopedia of Reagents for Organic Synthesis [online], Wiley & Sons, Published Online: 15 Apr 2006. DOI: 10.1002/047084289X.rn00665

52. Sherman, W.; Day, T.; Jacobson, M. P.; Friesner, R. A.; Farid, R. Novel procedure for modeling ligand/receptor induced fit effects. *J. Med. Chem.* **2006,** *49,* 534-553.

53. Ahn, K.; Boehm, M.; Brown, M. F.; Calloway, J.; Che, Y.; Chen, J.; Fennell, K. F.; Geoghegan, K. F.; Gilbert, A. M.; Gutierrez, J. A.; Kalgutkar, A. S.; Lanba, A.; Limberakis, C.; Magee, T. V.; O'Doherty, I.; Oliver, R.; Pabst, B.; Pandit, J.; Parris, K.; Pfefferkorn, J. A.; Rolph, T. P.; Patel, R.; Schuff, B.; Shanmugasundaram, V.; Starr, J. T.; Varghese, A. H.; Vera, N. B.; Vernochet, C.; Yan, J. Discovery of a selective covalent inhibitor of lysophospholipase-like 1 (LYPLAL1) as a tool to evaluate the role of this serine hydrolase in metabolism. *ACS Chem. Biol.* **2016,** *11,* 2529-2540.

54. Di, L.; Whitney-Pickett, C.; Umland, J. P.; Zhang, H.; Zhang, X.; Gebhard, D. F.; Lai, Y.; Federico, J. J., 3rd; Davidson, R. E.; Smith, R.; Reyner, E. L.; Lee, C.; Feng, B.; Rotter, C.; Varma, M. V.; Kempshall, S.; Fenner, K.; El-Kattan, A. F.; Liston, T. E.; Troutman, M. D. Development of a new permeability assay using low-efflux MDCKII cells. *J. Pharm. Sci.* **2011,** *100,* 4974-4985.

55. Obach, R. S.; Baxter, J. G.; Liston, T. E.; Silber, B. M.; Jones, B. C.; MacIntyre, F.; Rance, D. J.; Wastall, P. The prediction of human pharmacokinetic parameters from preclinical and in vitro metabolism data. *J. Pharmacol. Exp. Ther.* **1997,** *283,* 46-58.

56. Otwinowski, Z.; Minor, W. Processing of X-ray diffraction data collected in oscillation mode. *Methods Enzymol.* **1997,** *276,* 307-326.

57. Labar, G.; Bauvois, C.; Borel, F.; Ferrer, J. L.; Wouters, J.; Lambert, D. M. Crystal structure of the human monoacylglycerol lipase, a key actor in endocannabinoid signaling. *Chembiochem* **2010,** *11,* 218-227.

58. Bricogne G., B. E., Brandl M., Flensburg C., Keller P., Paciorek W., Roversi P, Sharff A., Smart O.S., Vonrhein C., Womack T.O. BUSTER version 2.11.5. **2016,** Cambridge, United Kingdom: Global Phasing Ltd.

59. Emsley, P.; Lohkamp, B.; Scott, W. G.; Cowtan, K. Features and development of Coot. *Acta Crystallogr. Sect. D. Biol. Crystallogr.* **2010,** *66,* 486-501.

Table of Content Graphic